



AMERICAN METEOROLOGICAL SOCIETY

Bulletin of the American Meteorological Society

EARLY ONLINE RELEASE

This is a preliminary PDF of the author-produced manuscript that has been peer-reviewed and accepted for publication. Since it is being posted so soon after acceptance, it has not yet been copyedited, formatted, or processed by AMS Publications. This preliminary version of the manuscript may be downloaded, distributed, and cited, but please be aware that there will be visual differences and possibly some content differences between this version and the final published version.

The DOI for this manuscript is doi: 10.1175/BAMS-D-17-0212.1

The final published version of this manuscript will replace the preliminary version at the above DOI once it is available.

If you would like to cite this EOR in a separate work, please use the following full citation:

Tian, H., J. Yang, C. Lu, R. Xu, J. Canadell, R. Jackson, A. Arneeth, J. Chang, G. Chen, P. Ciais, S. Gerber, A. Ito, Y. Huang, F. Joos, S. Lienert, P. Messina, S. Olin, S. Pan, C. Peng, E. Saikawa, R. Thompson, N. Vuichard, W. Winiwarter, S. Zaehle, B. Zhang, K. Zhang, and Q. Zhu, 2018: The global N₂O Model Intercomparison Project (NMIP): Objectives, Simulation Protocol and Expected Products. Bull. Amer. Meteor. Soc. doi:10.1175/BAMS-D-17-0212.1, in press.



The global N₂O Model Intercomparison Project (NMIP): Objectives, Simulation Protocol and Expected Products

Hanqin Tian^{1,2}, Jia Yang^{1,2}, Chaoqun Lu^{1,3}, Rongting Xu¹, Josep G Canadell⁴, Robert Jackson⁵, Almut Arneth⁶, Jinfeng Chang⁷, Guangsheng Chen^{1,2}, Philippe Ciais⁷, Stefan Gerber⁸, Akihiko Ito⁹, Yuanyuan Huang^{7,8}, Fortunat Joos^{10,11}, Sebastian Lienert^{10,11}, Palmira Messina⁷, Stefan Olin¹², Shufen Pan^{1,2}, Changhui Peng^{13,14}, Eri Saikawa¹⁵, Rona L. Thompson¹⁶, Nicolas Vuichard⁷, Wilfried Winiwarter^{17,18}, Sönke Zaehle¹⁹, Bowen Zhang¹, Kerou Zhang¹⁴, Qiuhan.Zhu¹⁴

¹ International Center for Climate and Global Change Research, School of Forestry and Wildlife Sciences, Auburn University, Auburn, AL 36849, USA

² Research Center for Eco-Environmental Sciences, Chinese Academy of Sciences, State Key Laboratory of Urban and Regional Ecology, Beijing 100085, China

³ Department of Ecology, Evolution, and Organismal Biology, Iowa State University, IA 50011, USA

⁴ Global Carbon Project, CSIRO Oceans and Atmosphere, Canberra, Australia

⁵ Department of Earth System Science, Woods Institute for the Environment, and Precourt Institute for Energy, Stanford University, Stanford, CA 94305-2210

⁶ Karlsruhe Institute of Technology, Institute of Meteorology and Climate Research/Atmospheric Environmental Research, 82467 Garmisch-Partenkirchen, Germany

⁷ Laboratoire des Sciences du Climat et de l'Environnement, LSCE, 91191 Gif sur Yvette, France

⁸ University of Florida, IFAS, Soil and Water Sciences Department, Gainesville, FL, 32611-0510, USA

⁹ Center for Global Environmental Research, National Institute for Environmental Studies, Tsukuba, 3058506, Japan

¹⁰ Climate and Environmental Physics, Physics Institute, University of Bern, Bern, Switzerland

¹¹ Oeschger Centre for Climate Change Research, University of Bern, Bern, Switzerland

¹² Department of Physical Geography and Ecosystem Science, Lund University, S-223 62 Lund, Sweden

¹³ Department of Biology Sciences, University of Quebec at Montreal (UQAM), Montréal (Québec), H3C 3P8, Canada

¹⁴ Center for Ecological Forecasting and Global Change, College of Forestry, Northwest A&F University, Yangling, Shaanxi 712100, China

¹⁵ Department of Environmental Sciences, Emory University, Atlanta, GA, USA

¹⁶ Norsk Institutt for Luftforskning - NILU, Kjeller, Norway

¹⁷ Air Quality and Greenhouse Gases (AIR), International Institute for Applied Systems Analysis, Schlossplatz 1A-2361 Laxenburg, Austria

¹⁸ The Institute of Environmental Engineering, University of Zielona Gora, Licealna 9, 65-417 Zielona Gora, Poland

¹⁹ Max Planck Institut für Biogeochemie, P.O. Box 600164, Hans-Knöll-Str. 10, 07745 Jena, Germany

Corresponding author: Hanqin Tian (tianhan@auburn.edu)

Bulletin of the American Meteorological Society (BAMS)

Revised Manuscript (12/26/2017)

43 **Abstract**

44 Nitrous oxide (N₂O) is an important greenhouse gas (GHG) and also an ozone-depleting
45 substance that has both natural and anthropogenic sources. Large uncertainty remains on the
46 magnitude and spatiotemporal patterns of N₂O fluxes and the key drivers of N₂O production in
47 the terrestrial biosphere. Some terrestrial biosphere models have been evolved to account for
48 nitrogen processes and show the capability to simulate N₂O emissions from land ecosystems at
49 the global scale, but large discrepancies exist among their estimates primarily due to inconsistent
50 input data sets, simulation protocol, and model structure and parameterization schemes. Based on
51 the consistent model input data and simulation protocol, the global N₂O Model Inter-Comparison
52 Project (NMIP) was initialized with ten state-of-the-art terrestrial biosphere models with N
53 cycling included. Specific objectives of NMIP are to: 1) Unravel the major N cycling processes
54 controlling N₂O fluxes in each model and identify the uncertainty sources from model structure,
55 input data and parameters; 2) Quantify the magnitude, spatial and temporal patterns of global and
56 regional N₂O fluxes from the pre-industrial period (1860) to present, and attribute the relative
57 contributions of multiple environmental factors to N₂O dynamics; and 3) Provide a bench-
58 marking estimate of N₂O fluxes through synthesizing the multi-model simulation results and
59 existing estimates from ground-based observations, inventories, and statistical and empirical
60 extrapolations. This study provides detailed descriptions for the NMIP protocol, input data,
61 model structure and key parameters, along with preliminary simulation results. The global and
62 regional N₂O estimation derived from the NMIP is a key component of the Global N₂O Budget
63 activity jointly led by the Global Carbon Project (GCP) and the International Nitrogen Initiative
64 (INI).

65

66
67
68
69
70
71
72
73
74
75
76
77
78
79
80
81
82
83
84
85
86
87
88

Capsules

The N₂O Model Inter-Comparison Project (NMIP) aims at understanding and quantifying the budgets of global and regional terrestrial N₂O fluxes, environmental controls and uncertainties associated with input data, model structure and parameters.

89 **1. Introduction**

90 Nitrous oxide (N₂O) is an important greenhouse gas and the time-integrated radiative
91 forcing resulting from a mass unit of N₂O is 298 times larger than that from carbon dioxide (CO₂)
92 emissions for a 100-year time horizon (Ciais et al., 2013; Myhre et al., 2013). Multiple lines of
93 evidence indicate that human activities (e.g., industrial N₂ fixation by the Haber-Bosch process
94 or by combustion, and manure N application) play an increasingly significant role in the
95 perturbation of the global N cycle (Galloway et al., 2008; Gruber et al., 2008; Fowler et al.,
96 2015), which has led to an increase in atmospheric N₂O concentration by ~21%, from 271 ppb at
97 pre-industrial level to 329 ppb in 2015 (MacFarling et al., 2006; Prather et al., 2012, 2015;
98 Thompson et al., 2014; <https://www.esrl.noaa.gov/>). The anthropogenic N₂O emissions are
99 estimated to have increased from 0.7 Tg N yr⁻¹ in 1860 to 6.9 Tg N yr⁻¹ in 2006, ~60% of which
100 was ascribed to agricultural activities (Ciais et al., 2013, Davidson and Kanter, 2014). The
101 increased N₂O emissions have significantly contributed to climate warming. During the 2000s,
102 the warming effect of N₂O emissions from the terrestrial biosphere counteracted more than half
103 of the cooling effect of the global land CO₂ sink (Tian et al., 2016), and anthropogenic N₂O
104 emissions are projected to lead to further global warming during the 21st century and beyond
105 (Stocker et al., 2013).

106 In terrestrial ecosystems, N₂O is mainly produced in soils via nitrification and
107 denitrification processes (Smith and Arah, 1990; Wrage et al., 2001; Schmidt et al., 2004). All
108 these processes are regulated by microbial activities under various soil micro-environments such
109 as soil temperature, moisture and aeration, clay content, pH, and C and N availability (Firestone
110 and Davidson, 1989; Goldberg and Gebauer, 2009; Butterbach-Bahl et al., 2013; Brotto et al.,
111 2015; Rowlings et al., 2015). In addition, N₂O emissions from terrestrial ecosystems can be

112 regulated by both natural disturbances and human management such as synthetic N fertilizer,
113 manure N application, irrigation, tillage, and the choice of crop varieties (Rice and Smith, 1982;
114 Cai et al., 1997; Ding et al., 2010). However, our understanding of the mechanisms responsible
115 for terrestrial N₂O emissions is still limited, which contributes to large uncertainties in estimating
116 both preindustrial and contemporary N₂O emissions. For example, estimates of global terrestrial
117 N₂O emissions from natural sources vary by up to a factor of three and range between 3.3 and
118 9.0 Tg N yr⁻¹ (Ciais et al. 2013). Human-induced biogenic N₂O emissions from the land
119 biosphere have not yet been investigated well (Tian et al. 2016). Therefore, a major international
120 and multidisciplinary effort is required to assess information from different research disciplines
121 and approaches in order to constrain current knowledge on the N₂O budget and drivers, and to
122 identify research gaps.

123 Process-based modeling is an essential tool in assessing and predicting the terrestrial N
124 cycle and N₂O fluxes in response to multi-factor global changes. Several process-based models
125 have been used to estimate N₂O emissions from natural and agricultural soils at various
126 spatiotemporal scales. The conceptual model of “hole-in-pipe” (Firestone and Davidson, 1989)
127 was first incorporated in the Carnegie-Ames-Stanford-Approach (CASA) Biosphere model
128 (Potter et al., 1993) to estimate N trace gas emissions at the global scale (Potter et al., 1996). The
129 daily version of the CENTURY model (DAYCENT) was linked to atmospheric models to better
130 estimate trace gas fluxes from different ecosystems (Parton et al., 1998). The DeNitrification-
131 DeComposition model (DNDC; Li et al., 1992) was developed to study the impacts of various
132 agricultural practices on N₂O emissions. In the Dynamic Land Ecosystem Model (DLEM), Tian
133 et al. (2011, 2015) considered the biotic and abiotic processes (e.g., plant N uptake and N
134 leaching loss) that regulate N₂O fluxes in natural and managed soils. In recent years, multiple C-

135 N coupled models, such as DyN-LPJ (Xu-Ri and Prentice, 2008), O-CN (Zaehle and Friend,
136 2010, 2011), Land Surface Processes and exchanges model of the University of Bern (LPX-Bern
137 1.0; Stocker et al., 2013), CLMCN-N₂O (Saikawa et al., 2014), and LM3V-N (Huang and Gerber,
138 2015) were developed by integrating a prognostic N cycle into different land surface models and
139 simulate N₂O emissions from land ecosystems. Unsurprisingly, these models generated divergent
140 estimates of global terrestrial N₂O budgets and spatiotemporal patterns mainly due to differences
141 in model input datasets, model structure, and parameterization schemes. What are the major
142 contributing factors responsible for the changing patterns of terrestrial N₂O emissions? How can
143 we narrow down the model-estimated bias or uncertainties? What are the knowledge gaps in
144 fully accounting for the N₂O processes? Here, we attempt to answer these questions through the
145 establishment and designing of the global N₂O Model Inter-comparison Project (NMIP).

146 During the past two decades, carbon-related Model Intercomparison Projects (MIPs) have
147 been established to evaluate model uncertainties in simulating the terrestrial carbon dynamics.
148 For example, the Vegetation-Ecosystem Modeling and Analysis Project (VEMAP) was a pioneer
149 MIP activity, driven by a common model input database and was established to provide multi-
150 model ensemble estimates of carbon fluxes and storage in response to changing climate and
151 atmospheric CO₂ (Melillo et al., 1995; Schimel et al., 2000). More recently, a number of CO₂-
152 oriented MIPs and synthesis activities were implemented, such as the North American Carbon
153 Program site and regional synthesis (NACP; Schwalm et al., 2010; Richardson et al., 2011;
154 Schaefer et al., 2012) and its extended Multi-Scale Synthesis and Terrestrial Model
155 Intercomparison Project (MsTMIP; Huntzinger et al., 2013; Wei et al., 2014), the TRENDY
156 Project (Le Quéré et al., 2016; Sitch et al., 2015), the Inter-Sectoral Impact Model
157 Intercomparison Project (ISI-MIP) (Warszawski et al., 2014; Ito et al., 2016), and the Multi

158 Model-data Synthesis of Terrestrial Carbon Cycles in Asia (Asia-MIP; Ichii et al., 2013). These
159 MIPs enhanced our understanding of model uncertainties and provided insight into future
160 directions of model improvement.

161 Following the CO₂-related MIPs, global methane (CH₄) MIPs and synthesis activities
162 were implemented in recent years, for example, the Wetland and Wetland CH₄ Intercomparison
163 of Models Project (WETCHIMP; Melton et al., 2013; Wania et al., 2013) and GCP global CH₄
164 budget synthesis (Sauniois et al., 2016; Poulter et al. 2017). Although terrestrial biogenic N₂O
165 emissions significantly contribute to climate warming, the model development for simulating N
166 cycle and N₂O fluxes remains far behind the CO₂- and CH₄-related activities. The relatively
167 sparse and short-term observations limited our understanding of N cycling in terrestrial
168 ecosystems. Comparing with CO₂ and CH₄, smaller N₂O concentration gradients in the
169 atmosphere and the varying magnitudes of soil N₂O emissions across observation sites and
170 periods makes it more difficult to quantify the N₂O budget at a large scale. Another important
171 uncertainty comes from the differences in model representation and parameterization schemes of
172 N processes, and the influence of biophysical and environmental factors on N₂O dynamics
173 (Appendix A). Similar to the purposes of the CO₂- and CH₄-related MIPs, there is a need to
174 initialize a MIP for the N models to assess the global N₂O budget. Under the umbrella of the
175 Global Carbon Project (GCP) and the International Nitrogen Initiative (INI), we initiated the
176 NMIP to investigate the uncertainty sources in N₂O estimates and provide multi-model N₂O
177 emissions estimates from natural and agricultural soils. This paper describes the detailed NMIP
178 protocol, input data, model structure, and some preliminary simulation results.

179

180 **2. The NMIP framework, objectives and tasks**

181 Motivated by large uncertainties and increasing data availability, the NMIP is developed
182 to establish a research network for providing a multi-model ensemble estimate on the
183 global/regional N₂O budgets and to identify major uncertainties associated with model structure,
184 parameters and input data (Figure 1). This project was first proposed at the Regional Carbon
185 Cycle Assessment and Processes (RECCAP) workshop “4th International workshop on Asian
186 Greenhouse Gases”, in JAMSTEC, Yokohama, Japan, April 8-10, 2014. The NMIP was
187 launched at a side meeting during the 2015 American Geophysical Union fall meeting and began
188 to work in the fall of 2016.

189 Specific objectives of NMIP are: 1) Unravel the major N cycling processes controlling
190 N₂O fluxes in each model and identify the uncertainty sources from modeling structure, input
191 data and parameters; 2) Quantify the magnitude, spatial and temporal patterns of global and
192 regional N₂O fluxes during 1860–2015, and attribute the relative contributions of multiple
193 environmental factors to N₂O dynamics; and 3) Provide a bench-mark estimate of global/regional
194 N₂O fluxes through synthesizing the multi-model simulation results and existing estimates from
195 ground-based observations, inventories, and statistical/empirical extrapolations. To achieve these
196 objectives, the NMIP group members have collectively developed a model simulation protocol
197 as outlined in Figure 1.

198 There are five key tasks or progressing stages in the protocol: 1) Development and
199 delivery of spatiotemporal model driving forces; 2) Individual model calibration and evaluation;
200 3) Model simulations and delivery of results; 4) Quality control and analysis of model results; 5)
201 Synthesis and uncertainty analysis.

202

203 **3. Key model input datasets**

204 To minimize the uncertainty that results from input datasets, the NMIP provided
205 consistent model driving datasets for all modeling groups. The datasets include potential
206 vegetation, climate, atmospheric CO₂ concentration, atmospheric N deposition, synthetic N
207 fertilizer applications in cropland and pasture, manure N production and applications in cropland
208 and pasture, and historical distribution of cropland at a spatial resolution of 0.5° by 0.5°
209 latitude/longitude (Table 1). Half-degree resolution is appropriate for studies at a global scale,
210 considering that most of model input data are available and many previous MIPs at a global scale
211 were conducted at this resolution. Here we briefly describe these input data sets and their
212 sources.

213 1) Climate: CRU-NCEP climate version 7 is a fusion of the CRU and NCEP/NCAR
214 reanalysis climate datasets between 1901 and 2015, which was reconstructed by the Laboratoire
215 des Sciences du Climat et l'Environnement, Paris, France (<https://vesg.ipsl.upmc.fr>). Major
216 climate variables include longwave and shortwave radiation, air pressure, humidity, temperature,
217 precipitation, and wind speed at 6-hourly temporal resolution. Monthly magnitude of climate
218 variables in CRU-NCEP dataset was forced to be consistent with the observational-based CRU
219 datasets.

220 2) Atmospheric CO₂: Monthly atmospheric CO₂ concentration from 1860 to 2015 was
221 obtained from NOAA GLOBALVIEW-CO₂ dataset derived from atmospheric and ice core
222 measurements (<https://www.esrl.noaa.gov>).

223 3) Vegetation: Potential vegetation map was acquired from the Synergetic Land Cover
224 Product (SYNMAP, <ftp://ftp.bgc-jena.mpg.de/pub/outgoing/mjung/SYNMAP/>), which merged
225 multiple satellite-global land cover maps into a desired classification approach (Jung et al., 2006).
226 Each 0.5° grid cell includes the area fractions for a maximum of 47 land cover types. Vegetation

227 in SYNMAP is classified according to its life form, leaf type, and leaf longevity. Barren ground,
228 permanent snow and ice are also included in this dataset. Based on this SYNMAP dataset,
229 participating model groups could create vegetated land fraction and reorganize the vegetation
230 types to generate the corresponding plant functional type and fractions for their models. Annual
231 cropland area from 1860 to 2015 was acquired from the HYDE 3.2 datasets
232 (<ftp://ftp.pbl.nl/hyde/>), which reconstructed time-dependent land use by historical population and
233 allocation algorithms with weighting maps (Klein Goldewijk et al., 2016). This dataset shows
234 that global cropland area increased from 5.9 million km² in the year of 1850 to 15.2 million km²
235 in the year of 2015.

236 4) Atmospheric N deposition onto land surface: The monthly atmospheric N deposition
237 (NH_x-N and NO_y-N) during 1860 - 2014 were from the IGAC/SPARC Chemistry-Climate
238 Model Initiative (CCMI) N deposition fields. CCMI models explicitly considered N emissions
239 from natural biogenic sources, lightning, anthropogenic and biofuel sources, and biomass
240 burning (Eyring et al., 2013). The transport of N gases has also been simulated by the chemical
241 transport module in CCMI models. This data was recommended by the Coupled Model
242 Intercomparison Project (CMIP) and used as the official products for CMIP6 models that lack
243 interactive chemistry components ([https://blogs.reading.ac.uk/ccmi/forcing-databases-in-support-](https://blogs.reading.ac.uk/ccmi/forcing-databases-in-support-of-cmip6/)
244 [of-cmip6/](https://blogs.reading.ac.uk/ccmi/forcing-databases-in-support-of-cmip6/)).

245 5) N fertilizer application: Spatially-explicit synthetic N fertilizer use data was
246 specifically developed in this project. We reconstructed the annual synthetic/mineral N fertilizer
247 dataset from 1960 to 2014 for the global cropland, matched with HYDE 3.2 cropland distribution
248 (Lu and Tian, 2017; <https://doi.pangaea.de/10.1594/PANGAEA.863323>). Data on national-level
249 crop-specific fertilizer use amount was collected from the International Fertilizer Industry

250 Association (IFA) and FAO. This N fertilizer dataset shows that the global total N fertilizer
251 amount increased from 11 Tg N yr⁻¹ in 1960 to 112 Tg N yr⁻¹ in 2013, and N fertilizer use rate
252 per unit cropland area increased by about 8 times in this period. N fertilizer application rate
253 before 1960 was linearly reduced to the zero in the 1900s.

254 6) Manure N production and application: Gridded annual manure N production in the
255 period of 1860-2014 was developed by integrating the Global Livestock Impact Mapping System
256 (GLIMS), the country-level livestock population from FAO, and N excretion rates of different
257 livestock categories according to IPCC 2006-Tier I and (Zhang et al., 2017,
258 <https://doi.org/10.1594/PANGAEA.871980>). This annual dataset shows that manure N
259 production increased by more than 6 times from 21 Tg N yr⁻¹ in 1860 to 131 Tg N yr⁻¹ in 2014,
260 and application rate of manure N to cropland is less than 20% of the total production. In this
261 project, we only consider the manure N application in cropland area. Manure N production and
262 application rates in 2015 was assumed to be same as that in 2014.

263 All the input datasets were delivered to the modeling groups in netCDF format. To fit
264 with individual modeling requirements for input datasets, the modeling groups could either use a
265 subset of these data sets or add some additional data sets. For example, the participating model
266 DLEM used all these environmental factors as inputs, while the model O-CN did not use manure
267 N as an input (See Table 3 for model input requirements in each model). Figure 2 illustrates the
268 inter-annual variations of the major input datasets at the global level during different available
269 time periods. Figure 3 shows the spatial patterns of atmospheric N deposition, N fertilizer use,
270 and manure N production in 1860, 1900, 1950, and 2014.

271

272 **4. Model result benchmarking and evaluation**

273 Except for bottom-up model simulations, the NMIP also plans to synthesize multiple
274 sources of terrestrial soil N₂O emission data to provide a benchmark for evaluating model
275 estimates. Four types of data will be collected or developed to serve as a potential benchmark: 1)
276 Site-level N cycling processes and N₂O emission measurements through chamber or eddy-flux
277 tower across biomes; 2) N₂O flux measurement data from national-based or global-based
278 measurement network (e.g., Long Term Ecological Research Network, Long Term
279 Agroecosystem Research Network, Greenhouse gas Reduction through Agriculture Carbon
280 Enhancement network, <http://www.n2o.net.au>, etc.) ; 3) Other spatialized datasets, including
281 statistical extrapolation (e.g., Xu et al. 2008; Kurokawa et al., 2013; Zhuang et al., 2012); 4) N₂O
282 fluxes from other than terrestrial ecosystem sources to allow for a global budget (industrial,
283 combustion, waste water & water bodies, marine and oceanic sources) (e.g., Battaglia and Joos,
284 in press; Davidson and Kanter, 2014; Galloway et al., 2004; Fowler et al., 2013; Winiwarter et
285 al., 2017); and 5) atmospheric inversions (e.g., Saikawa et al., 2014; Thompson et al., 2014) in
286 conjunction with atmospheric N₂O measurements from tall towers. We also call for more
287 observation-derived studies to provide regional and global N₂O emission estimates through
288 advanced computational techniques, such as machine learning, Multi-Tree Ensemble (MTE), and
289 remote sensing products. We anticipate that through multiple constraints, process-based
290 modeling approach can be more effective and reliable in estimating magnitude, spatial and
291 temporal patterns of terrestrial N₂O emissions, and quantifying relative contributions of
292 environmental drivers to N₂O dynamics.

293

294 **5. Major characteristics of participating models**

295 The N cycle in the earth system involves complex biogeochemical processes, in which N
296 is transformed into various chemical forms, and circulates among the atmosphere, terrestrial and
297 aquatic ecosystems. Important terrestrial processes in the N cycle include biological N fixation
298 (BNF), mineralization (conversion of organic N to inorganic N during the processes of organic
299 matter decomposition), immobilization (transformation of soil inorganic N to organic N),
300 ammonification (conversion of organic to ammonium N), volatilization (transformation of soil
301 ammonium N to ammonia gas), nitrification (transformation of ammonium N to nitrate and
302 nitrite N), denitrification (the process of nitrate reduction by microbial activities), plant uptake
303 from soil, resorption by living plant organs, adsorption and desorption by soil mineral particles,
304 and N leaching from soil to aquatic systems. The modeled N processes include N transformation
305 between organic and inorganic forms and movements among atmosphere, vegetation, soil, and
306 riverine systems. Although N processes are tightly coupled with carbon processes in soil and
307 vegetation, the greater variability in N processes compared to C processes make it more difficult
308 to simulate N cycling. At current stage, the NMIP has included ten ecosystem models with
309 explicit terrestrial N cycling processes (Table 2; Figure 1). Nine models (DLEM, LM3V-N,
310 ORCHIDEE, ORCHIDEE-CNP, O-CN, LPJ-GUESS, LPX-Bern, TRIPLEX-GHG and VISIT)
311 are capable of simulating N₂O emissions from both natural and agriculture ecosystems, while
312 one model (CLM-CN) only simulates N₂O emissions from natural vegetation. The biophysical
313 processes (such as, canopy structure, albedo and evapotranspiration), biogeochemical processes
314 (such as decomposition and denitrification), and N input for cropland are significantly different
315 from those for natural vegetation. For example, temperature in cropland was found to be lower
316 than that in natural forest due to the higher albedo and evapotranspiration (Bonan, 2000). These
317 differences could lead to different magnitude and timing of N₂O emissions from cropland.

318 Therefore, biophysical characteristics and management practices in cropland, such as crop
319 cultivation, fertilizer uses, irrigation and harvesting, are required to be explicitly represented by
320 the models with crop module.

321 In order to assess the uncertainty from model structure, each participating model was
322 asked to complete a detailed survey specifying the modeling mechanisms in exogenous N inputs
323 (e.g., N deposition, synthetic N fertilizer and manure N application, and BNF) and N
324 transformation processes. The summarized survey results are shown in Table 3. In general, N₂O
325 emissions from soil are regulated at two levels, which are the rates of nitrification and
326 denitrification in the soil and soil physical factors regulating the ratio of N₂O to other nitrous
327 gases (Davidson et al., 2000).

328 For N input to land ecosystems, all ten models considered the atmospheric N deposition
329 and biological fixation, nine models with a crop N₂O module included N fertilizer use, but only
330 six models considered manure as N input. For vegetation processes, all models included dynamic
331 algorithms in simulating N allocation to different living tissues and vegetation N turnover, and
332 simulated plant N uptake using the “Demand and Supply-driven” approach. For soil N processes,
333 all ten models simulated N leaching according to water runoff rate; however, the models differ in
334 representing nitrification and denitrification processes and the impacts of soil chemical and
335 physical factors. The differences in simulating nitrification and denitrification processes are one
336 of the major uncertainties in estimating N₂O emissions. Algorithms associated with N₂O
337 emissions in each participating model are briefly described in Appendix A.

338

339 **6. The NMIP model simulation methods and experimental designs**

340 **6.1 Model initialization**

341 The model simulations were divided into two stages: (1) spin-up and (2) transient runs
342 (Figure 4). During the spin-up run, models were driven by the repeated climate data from 1901 -
343 1920 and by other driving forces in 1860, i.e., atmospheric CO₂ concentration, N deposition, N
344 fertilizer use, manure N application, and land cover and land use change (LCLU). The N
345 fertilizer use was assumed to be zero in 1860. Each model group could determine the spin-up
346 running years according to model's specific requirement. For example, the DLEM assumed that
347 model reaches the equilibrium status when the differences of grid-level carbon, N, and water
348 stocks were less than 0.5 g C m⁻², 0.5 g N m⁻², and 0.5 mm in two consecutive 50 years. When
349 these thresholds were met, the spin-up run stopped and model reached an equilibrium state.

350

351 **6.2 Model simulation experiments**

352 During the transient run, seven experiments were designed to simulate global terrestrial
353 N₂O emissions. All the model experiments started with the equilibrium carbon, water and N
354 status in 1860, which is obtained from the spin-up run, and transiently ran through the period
355 during 1860-2015 (Figure 4). For the period of 1860-1900 when CRU/NCEP climate data is not
356 available, the 20-year average climate data between 1901 and 1920 were used. In the NMIP, we
357 applied the progressively reducing factor experimental scheme (i.e., first experiment includes all
358 factors and then reduce one factor each time; the effect of this factor is equal to the difference
359 between previous and current experiment) to simulate the impacts of individual environmental
360 factors on N₂O fluxes. In total, seven experiments (from S0 to S6) were designed (Figure 4). The
361 S0 reference (baseline) run was designed to track the model internal fluctuation and model drift.
362 The S1 experiment included the temporal variations of all time-varying driving forces. “Best
363 estimate” of N₂O emissions were acquired from either S1 experiment (for models considering

364 manure as input) or S2 experiment (for models without considering manure). The overall effect
365 of all environmental factors was calculated as: S1-S0. The effects of manure N use (MANN), N
366 fertilizer use (NFER), N deposition (NDEP), LCLU, atmospheric CO₂ (CO₂), and climate (CLIM)
367 were respectively calculated as: S1-S2, S2-S3, S3-S4, S4-S5, S5-S6, and S6-S0, respectively.

368

369 **7. Model outputs, quality control and data availability**

370 All participating model groups are requested to provide the gridded simulations of N₂O
371 fluxes from global terrestrial ecosystems and other relevant variables that can be used for
372 understanding C-N coupling and key N processes simulated by each individual model (Table 4).
373 The required model output will be submitted at the annual time-step during 1860-2015 and at the
374 monthly time-step during 1980-2015. In addition to modeling estimates of grid-level fluxes and
375 pool sizes, modeling groups will submit biome-level results to facilitate biome-level N₂O
376 emission analysis and split contributions of global N₂O dynamics to primary biome types. The
377 model output from each modeling group is sent to the core team led by Dr. Hanqin Tian for data
378 quality checking and preliminary analysis. The quality control is conducted to check if the
379 individual model results are reasonable and to avoid the obvious errors during model simulations.
380 After quality control process, model output is transferred to a data sharing website.

381 The model input and output datasets are made available to all model groups for further
382 analyses. Model input data and model results will be made available to broader research
383 community once the results of the first NMIP are published. A data use and authorship policy
384 has been established.

385

386 **8. Result analysis and synthesis**

387 Based on model results, the NMIP team will provide multi-model ensemble estimates for
388 terrestrial N₂O fluxes at various scales from country-, sector-, continental, to global, and also
389 assess differences and uncertainties among participating models. Through the seven simulation
390 experiments, the magnitudes and spatiotemporal variations in terrestrial N₂O emissions will be
391 attributed to changes in different environmental factors at both regional and global scales. The
392 global and regional N₂O flux data derived from other sources including atmospheric inversion,
393 statistical extrapolation, and inventory approaches (e.g., the N₂O emission data collected in Tian
394 et al. 2016) will be compared and integrated with the NMIP modeled results. Through these
395 syntheses and evaluations of modeled versus field observed N₂O dynamics, we will further
396 identify the gaps in our understanding to estimate N₂O fluxes and put forward potential strategies
397 to improve the models. In the following sections, we provide an initial analysis of simulated
398 terrestrial N₂O emissions from the three models (DLEM, O-CN, and VISIT), which simulate
399 both natural and agricultural emissions.

400 As indicated by the model ensemble, the global N₂O emission has significantly increased,
401 especially since the 1960s with more rapidly rising exogenous N inputs to terrestrial ecosystems
402 (Figure 5). Natural soils were the largest source across the entire period. Cropland is the single
403 largest contributor to the increasing trend in N₂O emissions during 1860-2015. Despite the same
404 input datasets, the interannual variations among the three models were different due to the
405 differences in model structure and parameters. The estimated N₂O emissions from VISIT were
406 consistently higher than those from the other two models during 1860-2015; N₂O emissions from
407 DLEM and O-CN were similar in magnitude. The increasing trends of N₂O emissions before the
408 end of 1960s were similar among the three models, while the largest increasing trend was found
409 for O-CN, followed by DLEM and the least for VISIT. The ultimate global terrestrial N₂O

410 budgets, interannual variations, and attributions of the differences among models will be further
411 analyzed in more detail after modeling results from all ten models are included.

412 The terrestrial N₂O emissions showed substantial spatial variations across the global land
413 surface since 1860 (Figure 6). The highest emission was from the tropical area during all four
414 periods (i.e., the 1860s, 1900s, 1950s, and 2001-2015) (Figure 6), primarily due to higher soil N
415 transformation rates and soil N contents in tropical ecosystems. The latitudinal distribution
416 patterns were slightly different from the 1860s to 2001-2015, showing an increasing importance
417 and second peak of N₂O emissions in the temperate climatic zone of the Northern Hemisphere.
418 Temperate regions were another hotspot for N₂O emissions due to the high N fertilizer use and N
419 deposition rates in China, India, Europe, and the contiguous United States. Of all 14 examined
420 regions as defined by Global Carbon Project (GCP) CH₄ budget synthesis (Saunio et al., 2016),
421 tropical South America had the largest N₂O emissions throughout the study period, contributing
422 to about 20% of the global total emission (Figure 7). China and the contiguous United States
423 were characterized by the most rapid N₂O increasing rates. In the recent three decades, China,
424 India, and western Europe were the only three regions with higher N₂O emissions from cropland
425 than that from natural ecosystems. It is noteworthy to point out that the estimated cropland N₂O
426 emissions in these three regions have large uncertainty ranges due to varied model representation
427 and parameterization methods of the impacts from agricultural management. Larger uncertainty
428 ranges for N₂O emissions from natural ecosystems were found in Russia, Northern Africa,
429 Boreal North America, Southeast Asia, and the contiguous United States.

430

431 **9. Summary**

432 Current assessments of terrestrial N₂O emission at regional and global scales are subject
433 to large uncertainties. The NMIP is attempting to better identify, and eventually reduce those
434 uncertainties. The activity was initialized in 2015 and currently includes ten terrestrial biosphere
435 models with N cycling coupled. NMIP is an open initiative and other models are invited to join
436 the effort. It targets to provide an improved estimate of global and regional terrestrial N₂O fluxes
437 as a contribution to the larger GCP Global N₂O Budget activity. NMIP is being developed with
438 the capacity to update flux estimates at regular intervals and quantify the uncertainties related to
439 model structure, algorithms, and parameters. The NMIP protocol includes seven simulation
440 experiments to quantify and attribute the contribution of environmental factors to the inter-
441 annual variation and long-term trend of terrestrial N₂O emissions. In addition, this project
442 intends to identify our knowledge gaps and bring forward potential strategies for improving the
443 prediction capability of N₂O models in the future. The data products and ensemble estimates of
444 terrestrial N₂O emissions will be made available and package to be relevant for policy makers
445 and non-government entities participating in the climate change issues.

446

447 **Acknowledgments**

448 H. Tian and his team acknowledge the support by National Key Research and Development
449 Program of China (# 2017YFA0604702), CAS Grants (KFJ-STZ-ZDTP-0; SKLURE2017-1-6),
450 NOAA Grants (G00010410, G00010318), National Science Foundation (1210360, 1243232) and
451 Auburn University IGP Program. A. Ito was supported by Japan Society for the Promotion of
452 Science (Grant # 17H01867). C. Peng acknowledges the support by National Science and
453 Engineering Research Council of Canada (NSERC) discovery grant and China's QianRen
454 Program. E. Saikawa was supported by NOAA Climate Program Office's AC4 program, award #

455 NA13OAR4310059. S. Zaehle was supported by the European Research Council (ERC) under
456 the European Union’s H2020 Programme (grant # 647304; QUINCY). P. Ciais and J. Chang are
457 supported by the European Research Council Synergy grant ERC-2013-SyG-
458 610028 IMBALANCE-P. S. Lienert and F. Joos acknowledge support by the Swiss National
459 Science Foundation (# 200020_172476). We acknowledge Dr. Andy Jacobson for extending
460 global gridded monthly CO₂ data for us to use in the NMIP. The authors declare no conflict of
461 interest.

462

463 **Appendix A: Brief description of algorithms associated with N₂O flux in each participating**
464 **model**

465 1) CLM-CN-N₂O:

466 CLMCN-N₂O is based on the DeNitrification-DeComposition (DNDC) model (Li et al.,
467 1992) implemented in the Community Land Model v3.5 (Oleson et al., 2008; Stöckli et al., 2008)
468 with explicit carbon and nitrogen (CN) processes (Thornton et al., 2007; Randerson et al., 2009;
469 Thornton et al. 2009). CLMCN-N₂O is added to CLM-CN v3.5 in a one-way coupling
470 framework and simulates N₂O emissions during nitrification and denitrification processes at an
471 hourly time step.

472 Nitrification (R_{nit}) is temperature and moisture dependent and N₂O is computed by the
473 following equation as described in Li et al. (1992):

$$474 R_{nit} = C_{NH_4} f(T1) \tag{1}$$

475 where C_{NH_4} is the NH₄⁺-N content in soil and $f(T1)$ is the response function of soil temperature
476 to nitrification rate.

477 Denitrification is also soil temperature and moisture dependent and it takes place under
 478 the anaerobic state. CLMCN-N₂O specifies the anaerobic state when the water-filled pore space
 479 is more than 41.5% in the soil layer. Under this condition, N₂O is created based on the growth
 480 rate of denitrifying bacteria, as well as consumption and assimilation by plants and microbes,
 481 following Li et al. (1992). Detailed processes in simulating N₂O emissions can be found in
 482 Saikawa et al., 2013.

483

484 2) DLEM2.0:

485 The nitrogen cycle scheme in DLEM2.0 (Yang et al. 2015; Xu et al. 2017) are similar as
 486 DLEM1.0 (Tian et al., 2010, 2011, 2012; Lu and Tian., 2013; Xu et al., 2012), However, the
 487 N₂O emission schemes in DLEM2.0 (Xu et al., 2017) have been modified based on Chatskikh et
 488 al. (2005) and Heinen (2006).

$$489 \quad R_{nit} = k_{nit_max} f(T1) f(WFPS) C_{NH4} \quad (2)$$

$$490 \quad R_{den} = k_{den_max} f(T2) f(WFPS) C_{NO3} \quad (3)$$

491 where R_{nit} is the daily nitrification rate (g N/m²/d); R_{den} is the daily denitrification rate (g
 492 N/m²/d); $f(T1)$ and $f(T2)$ are the impact function of daily soil temperature on nitrification and
 493 denitrification, respectively; $f(WFPS)$ is the impact function of water-filled pore space (WFPS)
 494 on nitrification, denitrification and N₂O diffusion; k_{nit_max} is the maximum fraction of NH₄⁺-N
 495 that is converted to NO₃⁻-N or gases (0-1); k_{den_max} is the maximum fraction of NO₃⁻-N that is
 496 converted to gases (0-1); C_{NH4} and C_{NO3} are the soil NH₄⁺-N and NO₃⁻-N content (g N/m²). N₂O
 497 from denitrification and nitrification processes are calculated as,

$$498 \quad R_{N2O} = (R_{nit} + R_{den}) f(T3) (1 - f(WFPS)) \quad (4)$$

499 where R_{N_2O} is the daily N_2O emission rate ($g\ N/m^2/d$); $f(T3)$ is the impact function of daily soil
 500 temperature on N_2O diffusion rate from soil pores. The calculation methods for these functions
 501 and parameters were described in detail in Xu et al. (2017) and Yang et al. (2015).

502

503 3) LM3V-N:

504 In LM3V-N, nitrification is proportional to substrate availability (i.e., NH_4^+), modified by
 505 functions that account for effects of temperature and WFPS adapted from Parton et al. (1996).

506 Nitrification-associated N_2O emission (R_{nit}) is evaluated by

$$507 R_{nit} = k_{nit_base} f(WFPS) f(T1) C_{NH_4} / b_{NH_4} \quad (5)$$

508 where k_{nit_base} is the base nitrification rate; b_{NH_4} is the buffer parameter for soil NH_4^+ .

509 Denitrification is described by a Monod-type equation, where both carbon and nitrate
 510 substrate availability can have limiting effects on N gas production following Li et al. (2000).
 511 These functions are further modified by temperature (based on Xu-Ri and Prentice, 2008), and
 512 by WFPS indicating the availability and/or absence of oxygen (adapted from Parton et al., 1996).

$$513 R_{den} = k_{den_base} f(T2) f(WFPS) f_g C_{NO_3} / b_{NO_3} \quad (6)$$

514 where k_{den_base} is the base denitrification rate; f_g denotes the impact of labile carbon availability
 515 to nitrate on the growth of denitrifies; b_{NO_3} is the buffer parameter for soil NO_3^- .

516 Gaseous losses are partitioned between NO_x and N_2O during nitrification is
 517 parameterized based on air-filled porosity, following Parton et al. (2001). Partitioning between
 518 N_2O and N_2 during denitrification follows the empirical function of Del Grosso et al. (2000),
 519 which combines effects of substrate, electron donors (labile C), and water filled pore space.

$$520 R_{N_2O} = 0.004 R_{nit} + R_{den} f(WFPS) f(C_{NO_3}) \quad (7)$$

521 Nitrification/denitrification are treated as fast processes (Shevliakova et al., 2009) and
522 thus updated on sub-hourly time steps along with updates on soil moisture, soil temperature and
523 C and N mineralization. Model description including model formulation are detailed in Huang
524 and Gerber (2015).

525

526 4) LPJ-GUESS:

527 The nitrogen cycle scheme in LPJ-GUESS is based on CENTURY (Parton et al., 1996)
528 and Xu-Ri and Prentice (2008). Inorganic soil nitrogen pools in the model are: ammonium,
529 nitrite and nitrate. Nitrification only occurs in the dry part of the soil (fractionated using water-
530 filled pore space, WFPS), the ratio between N_2O and NO_x of the gaseous losses in nitrification is
531 based on the moisture content in the soil ($f(WFPS)$).

$$532 R_{nit} = k_{nit_max} f(WFPS) C_{NH4} \quad (8)$$

533 Denitrification occurs in the wet part (based on WFPS) of the soil, the denitrification rate
534 depends on temperature, soil moisture and labile carbon (approximated with heterotrophic
535 respiration, rh). Gaseous losses through denitrification results in N_2O , N_2 and NO_x .

$$536 R_{den} = k_{den_base} f(T2) f(WFPS) f(rh) C_{NO3} \quad (9)$$

537 The fractionation between the gaseous N species are modelled using soil moisture and
538 temperature. All losses of gaseous N, are modelled. Emissions to the atmosphere from these
539 pools are modelled using rate modifiers that are based on the soil moisture and temperature. No
540 re-transformation of these gaseous N species is considered. These processes (N-cycling and
541 gaseous N emissions) are modelled in different land use classes: natural vegetation,
542 pastures/rangelands and croplands. On croplands, fertilizers are spread as mineral and/or organic
543 N. Mineral fertilizers are considered as an input to the ammonium and nitrate pools at a fixed

544 ratio (50/50), and manure as an input into the organic nitrogen pool with a fixed C:N ratio
545 (currently set to 30).

546

547 5) LPX-Bern:

548 The implementation of nitrogen dynamics in LPX-Bern is based on the work of Xu-Ri
549 and Prentice (2008). Nitrogen uptake by plants is governed by their demand and the availability
550 of nitrogen in two soil pools representing ammonium and nitrate. Nitrogen from deposition and
551 fertilization are added to these inorganic soil pools. Losses include ammonium volatilization,
552 nitrate leaching as well as N₂O and NO production during nitrification and N₂O, NO and N₂
553 production during denitrification. Aerobic nitrification of ammonium is dependent on soil
554 temperature (T_{soil}) and indirectly on soil water content due to the partitioning of wet and dry soil:

$$555 R_{nit} = max_{nit} f_1(T_{soil}) C_{NH_4, dry} \quad (10)$$

556 where $max_{nit} = 0.92 \text{ day}^{-1}$ is the daily maximum nitrification rate at 20°C.

557 Anaerobic denitrification of nitrate in wet soil depends on labile carbon availability and soil
558 temperature:

$$559 R_{den} = R_{mb} / (R_{mb} + K_{mb}) f_2(T_{soil}) C_{NO_3, wet} / (C_{NO_3, wet} + K_n) \quad (11)$$

560 The parameters K_{mb} and K_n are taken from Xu-Ri and Prentice (2008) and R_{mb} is the
561 microbiological soil respiration. The amount of Nitrogen lost as N₂O due to nitrification and
562 denitrification is modelled as a function of soil temperature, water content and the respective
563 process rate.

564

565 6) O-CN:

566 The treatment of inorganic soil nitrogen dynamics in O-CN follows largely Xu-Ri and

567 Prentice (2008). O-CN (Zaehle and Friend, 2010) considers N losses to NH₃ volatilisation, NO_x,
 568 N₂O and N₂ production and emission, as well as NH₄ and NO₃ leaching. Inorganic nitrogen
 569 dynamics in the soil are tightly coupled to plant uptake and net mineralization. The anaerobic
 570 volume fraction of the soil is estimated by an empirical function of the fractional soil moisture
 571 content (Zaehle et al. 2011). The fraction of ammonium in the aerobic part of the soil is subject
 572 to nitrification, according to:

$$573 \quad R_{nit} = v_{max_{nit}} f(T1) f(pH1) C_{NH4} \quad (12)$$

574 where $f(pH1)$ is the soil pH response functions for nitrification (Li et al. 1992; Xu-Ri and
 575 Prentice, 2008), and $v_{max_{nit}}$ is the maximum daily nitrification rate under 20°C and favourable
 576 pH conditions (Xu-Ri and Prentice, 2008).

577 Gross denitrification of the fraction of nitrate under anoxic conditions is modelled as:

$$578 \quad R_{den} = R_{mb} / (R_{mb} + K_{mb}) f(T2) f(pH2) C_{NO3} / (C_{NO3} + K_n) \quad (13)$$

579 where $f(pH2)$ is the soil pH response functions for denitrification (Li et al., 1992; Xu-Ri and
 580 Prentice, 2008), R_{mb} is the soil microbial respiration rate, and K_{mb} and K_n parameters taken from
 581 Li et al. (1992).

582 The N₂O production from nitrification and denitrification is then calculated as:

$$583 \quad R_{N2O} = a_{nit} f(T1) R_{nit} + b_{den} f(T2) f(pH3) R_{den} \quad (14)$$

584 where a_{nit} and b_{den} are fraction loss constants, $f(pH3)$ is a pH-modifier changing the degree of
 585 denitrification producing N₂O versus NO_x or N₂ (Zaehle et al. 2011). Emissions of volatile
 586 compounds are simulated using the empirical emission of Xu-Ri and Prentice (2008).

587

588 7) ORCHIDEE:

589 Modeling of the mineral N dynamics by the ORCHIDEE model originates from the
 590 formulations used in the O-CN (Zaehle and Friend, 2010). It is composed of five pools for
 591 ammonium/ammoniac, nitrate, NO_x, nitrous oxide, and di-nitrogen forms. N₂O production in
 592 both nitrification and denitrification processes are represented.

593 The potential daily rate of nitrification, R_{nit} , occurs only on the aerobic fraction of the
 594 soil and is a function of temperature, pH, and ammonium concentration (C_{NH4}):

$$595 R_{nit} = (1 - f(WFPS))f(T1)f(pH1)k_{nit}C_{NH4} \quad (15)$$

596 where k_{nit} is the reference potential NO₃⁻ production per mass unit of ammonium.

597 N₂O production by nitrification ($R_{N2O,nit}$, g N-N₂O/m²/d) is expressed as a function of the
 598 potential daily rate of nitrification (R_{nit} , g N-NO₃⁻/m²/d), temperature and the water content as
 599 shown in Zhang et al. (2002).

$$600 R_{N2O,nit} = f(WFPS)f(T1)R_{nit}p_{N2O,nit} \quad (16)$$

601 where $p_{N2O,nit}$ (g N-N₂O (g N-NO₃⁻)⁻¹) is the reference N₂O production per mass unit of NO₃⁻
 602 produced by nitrification. The denitrification occurs on the anaerobic fraction of the soil which is
 603 computed as a function of the water-filled porosity ($f(WFPS)$) and is controlled by temperature,
 604 pH, soil NO concentration and denitrifier microbial activity (a_{microb} , g m⁻²) (Li et al., 2000).

$$605 R_{N2O,den} = f(WFPS)f(T2)f(pH)f(NO)p_{N2O,den}a_{microb} \quad (17)$$

606 where $f(NO)$ is a Michaelis-Menten shape function and $p_{N2O,den}$ is the reference N₂O production
 607 per mass unit of denitrifier microbes.

608

609 8) ORCHIDEE-CNP

610 ORCHIDEE-CNP (Goll et al., 2017) is a version with the implementation of the
 611 phosphorus cycle into the nitrogen enabled version of ORCHIDEE (ORCHIDEE-CN; Vuichard

612 in prep.). The inorganic soil nitrogen dynamics of ORCHIDEE-CNP includes N₂O from both
613 nitrification and denitrification processes following the processes of O-CN (Zaehle et al., 2011).
614 One exception is the BNF. In ORCHIDEE-CNP, BNF is a function of NPP (Cleveland et al.,
615 1999) and also regulated by soil mineral N concentration. ORCHIDEE-CNP accounts for
616 influence of phosphorus state of vegetation on tissue nutrient concentrations and phosphatase-
617 mediated biochemical mineralization. Changes in nutrient content (quality) of litter affect the
618 carbon use efficiency of decomposition and in return the nutrient availability to vegetation. The
619 model explicitly accounts for root zone depletion of phosphorus as a function of root phosphorus
620 uptake and phosphorus transport from soil to the root surface.

621

622 9) TRIPLEX-GHG

623 TRIPLEX-GHG model (Zhu et al., 2014; Zhang et al., 2017) is designed to simulate N₂O
624 emissions by coupling major theoretical foundations for processes of nitrification and
625 denitrification reported by Li et al. (2000). Briefly, the nitrification rate is calculated by the
626 Michaelis-Menten function based on the concentration of NH₄⁺, and microbial activity of
627 nitrifying bacteria is explicitly involved based on simulating their growth and death;
628 denitrification is expressed in a more complex way by taking into account the chain reaction
629 ($NO_3^- \rightarrow NO_2^- \rightarrow NO \rightarrow N_2O \rightarrow N_2$). Each step of denitrification can be regarded as an
630 independent process, but these steps are linked by competition for DOC between specific
631 denitrifiers during each step. A double substrate-based (DOC and NO_x) Michaelis-Menten
632 equation was adopted to simulate the growth rates of NO_x denitrifiers (Li et al., 2000). In
633 addition, the effects of different factors, such as soil temperature, soil moisture and pH, are also
634 considered. The key equations for nitrification are showed as follows,

635 $R_{nit} = B_{nit} \frac{R_{max} C_{NH_4}}{(6.18 + C_{NH_4})} pH$ (18)

636 $R_{max} = COE_{NR} \cdot N_p$ (19)

637 $F_{NN_2O} = FMAX_{N_2O} R_{nit} f(T1) f(WFPS)$ (20)

638 where R_{nit} is the nitrification rate ($\text{kg N m}^{-2} \text{d}^{-1}$); R_{max} is the maximum nitrification rate (d^{-1}); B_{nit}
 639 is the biomass concentration of nitrifiers (kg C m^{-2}); pH is the soil pH; COE_{NR} represents the
 640 nitrification coefficient; N_p represents the nitrification potential ($\text{mg N kg}^{-1} \text{d}^{-1}$); $FMAX_{N_2O}$ is the
 641 maximum N_2O fraction during nitrification ($\text{kg N m}^{-2} \text{d}^{-1}$); and $f(T1)$ and $f(WFPS)$ are the
 642 functions of the effects of soil temperature and soil moisture on N_2O emissions during
 643 nitrification, respectively.

644 The key equations for denitrification are showed as follows,

645 $R_{NO_x} = MUE_{NO_x} \frac{[DOC]}{[DOC] + K_c} \frac{[NO_x]}{[NO_x] + K_n}$ (21)

646 $F_{ANNO_x} = COE_{dNO_x} B_{denit} \left(\frac{R_{NO_x}}{EFF_{NO_x}} + \frac{MAI_{NO_x} [NO_x]}{[N]} \right) f_{NO_x}(pH2) f(T2)$ (22)

647 where MUE_{NO_x} is the maximum growth rate of NO_x denitrifiers (h^{-1}); $[DOC]$ and $[NO_x]$ represent
 648 the concentrations of DOC ($\text{kg C m}^{-3} \text{h}^{-1}$) and NO_x ($\text{kg N m}^{-3} \text{h}^{-1}$), respectively, in the anaerobic
 649 balloon; K_c (kg C m^{-3}) and K_n (kg N m^{-3}) are the half saturation value of C and N oxides,
 650 respectively. F_{ANNO_x} is the consumption rate of NO_x ($\text{kg N m}^{-3} \text{h}^{-1}$); COE_{dNO_x} represents the
 651 coefficient of NO_x consumption; B_{denit} is the biomass of denitrifiers (kg C m^{-3}); R_{NO_x} is the NO_x
 652 reduction rate (h^{-1}); $[NO_x]$ and $[N]$ are the concentrations of NO_x and total N, respectively, in the
 653 anaerobic balloon (kg N m^{-3}); EFF_{NO_x} is the efficiency parameter for NO_x denitrifiers (kg C kg N
 654 $^{-1}$); MAI_{NO_x} is the maintenance coefficient of NO_x (h^{-1}); and $f(t)_{denit}$ represents the effect of the
 655 soil temperature on the denitrification rate during each step.

656

657 10) VISIT

658 The nitrogen cycle scheme of VISIT is composed of three organic soil nitrogen pools
659 (microbe, litter, and humus), two inorganic soil nitrogen pools (ammonium and nitrate), and
660 vegetation pools. Fertilizer is considered as an input to the ammonium and nitrate pools at a
661 fixed ratio, and manure as an input into the litter organic nitrogen pool. N₂O emissions through
662 nitrification and denitrification are estimated using the scheme developed by Parton et al. (1996).
663 Nitrification-associated N₂O emission (R_{nit,N_2O}) is evaluated as follows,

$$664 R_{nit,N_2O} = f(WFPS)f(pH1)f(T1)(K_{max} + F_{max}f(NH_4)) \quad (23)$$

665 where K_{max} is the soil-specific turnover coefficient; F_{max} is the parameter of maximum
666 nitrification gas flux; and $f(NH_4)$ is the effect of soil ammonium on nitrification. Denitrification-
667 associated N₂O emission (R_{den,N_2O}) is evaluated by the following equation:

$$668 R_{den,N_2O} = R_{den}(1 + R_{N_2/N_2O}) \quad (24)$$

$$669 R_{den} = \min(f(NO_3), f(CO_2)) \times f(WFPS) \quad (25)$$

670 where R_{N_2/N_2O} is the fractionation coefficient, which is also a function of WFPS, soil nitrate, and
671 heterotrophic respiration, $f(NO_3)$ is the maximum denitrification rate in high soil respiration
672 rate condition, $f(CO_2)$ is the maximum denitrification rate in high NO₃⁻ levels, and $f(WFPS)$ is
673 the effect of WFPS on denitrification rate.

674

675

676 **References**

- 677 Battaglia, G. and Joos, F. In PRESS: Marine N₂O emissions from nitrification and denitrification
678 constrained by modern observations and projected in multi-millennial global warming
679 simulations. *Global Biogeochemical Cycles*. DOI: 10.1002/2017GB005671 Bonan, G. B.
680 2001: Observational evidence for reduction of daily maximum temperature by croplands in
681 the Midwest United States. *Journal of Climate*, 14(11), 2430-2442.
- 682 Brotto, A. C., Kligerman, D. C., Andrade, S. A., Ribeiro, R. P., Oliveira, J. L., Chandran, K., and
683 de Mello, W. Z., 2015: Factors controlling nitrous oxide emissions from a full-scale activated
684 sludge system in the tropics, *Environmental Science and Pollution Research*, 22, 11840-
685 11849.
- 686 Butterbach-Bahl, K., Baggs, E. M., Dannenmann, M., Kiese, R., and Zechmeister-Boltenstern, S.,
687 2013: Nitrous oxide emissions from soils: how well do we understand the processes and their
688 controls?, *Philosophical Transactions of the Royal Society B*, 368, 20130122,
689 <https://doi.org/10.1098/rstb.2013.0122>.
- 690 Cai, Z., Xing, G., Yan, X., Xu, H., Tsuruta, H., Yagi, K., and Minami, K., 1997: Methane and
691 nitrous oxide emissions from rice paddy fields as affected by nitrogen fertilisers and water
692 management, *Plant and soil*, 196, 7-14.
- 693 Chatskikh, D., Olesen, J. E., Berntsen, J., Regina, K., and Yamulki, S., 2005: Simulation of
694 effects of soils, climate and management on N₂O emission from grasslands, *Biogeochemistry*,
695 76, 395-419.
- 696 Ciais, P., and Coauthors, 2013: Carbon and other biogeochemical cycles. In *Climate Change*
697 2013: The Physical Science Basis. Contribution of Working Group I to the Fifth Assessment
698 Report of the Intergovernmental Panel on Climate Change, Cambridge University Press,
699 Cambridge, UK, 465–570.
- 700 Cleveland, C. C. and Coauthors, 1999: Global patterns of terrestrial biological nitrogen (N₂)
701 fixation in natural ecosystems, *Global Biogeochemical Cycles*, 13, 623-645.
- 702 Davidson, E. Keller, M., Erickson, H., Verchot, L., and Veldkamp, E., 2000: Testing a
703 conceptual model of soil emissions of nitrous and nitric oxides: using two functions based on
704 soil nitrogen availability and soil water content, the hole-in-the-pipe model characterizes a
705 large fraction of the observed variation of nitric oxide and nitrous oxide emissions from soils.
706 *AIBS Bulletin* 50, 8(2000), 667-680.

707 Davidson, E. A., 2009: The contribution of manure and fertilizer nitrogen to atmospheric nitrous
708 oxide since 1860, *Nature Geoscience*, 2, 659-662.

709 Davidson, E. A. & Kanter, D., 2014: Inventories and scenarios of nitrous oxide emissions.
710 *Environ. Res. Lett.* 9, 105012.

711 Del Grosso, S., Parton, W., Mosier, A., Ojima, D., Kulmala, A., and Phongpan, S., 2000:
712 General model for N₂O and N₂ gas emissions from soils due to denitrification, *Global*
713 *Biogeochemical Cycles*, 14, 1045-1060.

714 Ding, W., Yagi, K., Cai, Z., and Han, F., 2010: Impact of long-term application of fertilizers on
715 N₂O and NO production potential in an intensively cultivated sandy loam soil, *Water, Air, &*
716 *Soil Pollution*, 212, 141-153.

717 Eyring, Veronika and Coauthors, 2013: Overview of IGAC/SPARC Chemistry-Climate Model
718 Initiative (CCMI) community simulations in support of upcoming ozone and climate
719 assessments, *SPARC newsletter* 40(Januar): 48-66.

720 Firestone, M. K. and Davidson, E. A., 1989: Microbiological basis of NO and N₂O production
721 and consumption in soil, *Exchange of trace gases between terrestrial ecosystems and the*
722 *atmosphere*, 47, 7-21.

723 Fowler, D. and Coauthors, 2013: The global nitrogen cycle in the twenty-first century.
724 *Philosophical Transactions of the Royal Society B: Biological Sciences*, 368, 20130164–
725 20130164. <https://doi.org/10.1098/rstb.2013.0164>

726 Fowler, D. and Coauthors, 2015: Effects of global change during the 21st century on the nitrogen
727 cycle, *Atmospheric Chemistry and Physics*, 15(24), 13849-13893.

728 Galloway, J. N. and Coauthors, 2004: Nitrogen Cycles: Past, Present, and Future.
729 *Biogeochemistry* 70: 153–226

730 Galloway, J. N. and Coauthors, 2008: Transformation of the nitrogen cycle: recent trends,
731 questions, and potential solutions, *Science*, 320, 889-892.

732 Goldberg, S. D. and Gebauer, G., 2009: Drought turns a Central European Norway spruce forest
733 soil from an N₂O source to a transient N₂O sink, *Global Change Biology*, 15, 850-860.

734 Goll, D. S. and Coauthors, 2017: A representation of the phosphorus cycle for ORCHIDEE,
735 *Geoscientific Model Development Discussion*, <https://doi.org/10.5194/gmd-2017-62>, in
736 review.

737 Gruber, N. and Galloway, J. N., 2008: An Earth-system perspective of the global nitrogen cycle,
738 Nature, 451, 293-296.

739 Heinen, M., 2006: Simplified denitrification models: overview and properties, *Geoderma*, 133,
740 444-463.

741 Huang, Y. and Gerber, S., 2015: Global soil nitrous oxide emissions in a dynamic carbon-
742 nitrogen model, *Biogeosciences*, 12, 6405-6427.

743 Huntzinger, D. N. and Coauthors, 2013: The North American Carbon Program Multi-scale
744 Synthesis and Terrestrial Model Intercomparison Project: Part 1: Overview and experimental
745 design, *Geoscientific Model Development*, 6, 2121–2133, [http://doi.org/10.5194/gmd-6-](http://doi.org/10.5194/gmd-6-2121-2013)
746 2121-2013.

747 Ichii, K. and Coauthors, 2013: Site-level model–data synthesis of terrestrial carbon fluxes in the
748 CarboEastAsia eddy-covariance observation network: toward future modeling efforts,
749 *Journal of Forest Research*, 18, 13-20.

750 Inatomi, M., Ito, A., Ishijima, K., and Murayama, S., 2010: Greenhouse gas budget of a cool-
751 temperate deciduous broad-leaved forest in Japan estimated using a process-based model,
752 *Ecosystems*, 13, 472-483.

753 Ito, A. and Inatomi, M., 2012: Use of a process-based model for assessing the methane budgets
754 of global terrestrial ecosystems and evaluation of uncertainty, *Biogeosciences*, 9, 759-773

755 Ito, A., Nishina, K., and Noda, H. M., 2016: Evaluation of global warming impacts on the carbon
756 budget of terrestrial ecosystems in monsoon Asia: a multi-model analysis, *Ecological*
757 *research*, 31, 459-474.

758 Jung, M., Henkel, K., Herold, M., and Churkina, G., 2006: Exploiting synergies of global land
759 cover products for carbon cycle modeling, *Remote Sensing of Environment*, 101, 534-553.

760 Klein Goldewijk, K., Beusen, A., Doelman, J., and Stehfest, E., 2016: New anthropogenic land
761 use estimates for the Holocene; HYDE 3.2, *Earth System Science Data Discussions*,
762 <https://doi.org/10.5194/essd-2016-58>, in review.

763 Kurokawa, J., Ohara, T., Morikawa, T., Hanayama, S., Janssens-Maenhout, G., Fukui, T.,
764 Kawashima, K., and Akimoto, H. 2013: Emissions of air pollutants and greenhouse gases
765 over Asian regions during 2000–2008: Regional Emission inventory in ASia (REAS) version
766 2. *Atmospheric Chemistry and Physics*, 21, 11019-11058.

767 Le Quéré, C. and Coauthors, 2016: Global carbon budget 2016, *Earth System Science Data*, 8,
768 605-649.

769 Li, C., Aber, J., Stange, F., Butterbach-Bahl, K., Papen, H., Zechmeister-Boltenstern, S., Li, C.
770 S., and Aber, J., 2000: A process-oriented model of N₂O and NO emissions from forest soils:
771 1. Model development, *Journal of Geophysical Research: Atmospheres*, 105, 4369-4384.

772 Li, C., Frohling, S., and Frohling, T. A., 1992: A model of nitrous oxide evolution from soil
773 driven by rainfall events: 1. Model structure and sensitivity, *Journal of Geophysical Research:*
774 *Atmospheres*, 97, 9759-9776.

775 Lu, C. and Tian, H., 2017: Global nitrogen and phosphorus fertilizer use for agriculture
776 production in the past half century: shifted hot spots and nutrient imbalance, *Earth System*
777 *Science Data*, 9, 181-192.

778 Lu, C. and Tian, H., 2013: Net greenhouse gas balance in response to nitrogen enrichment:
779 perspectives from a coupled biogeochemical model, *Global Change Biology*, 19, 571-588.

780 Lü, C. and Tian, H., 2007: Spatial and temporal patterns of nitrogen deposition in China:
781 synthesis of observational data, *Journal of Geophysical Research: Atmospheres*, 112,
782 D22S05, <http://doi.org/10.1029/2006JD007990>.

783 MacFarling, M. and Coauthors, 2006: Law Dome CO₂, CH₄ and N₂O ice core records extended
784 to 2000 years BP. *Geophysical Research Letters*, 33. L14810.

785 Melillo, J., Borchers, J., and Chaney, J., 1995: Vegetation/ecosystem modeling and analysis
786 project: Comparing biogeography and geochemistry models in a continental-scale study of
787 terrestrial ecosystem responses to climate change and CO₂ doubling, *Global Biogeochemical*
788 *Cycles*, 9, 407-437.

789 Melton, J. and Coauthors, 2013: Present state of global wetland extent and wetland methane
790 modelling: conclusions from a model intercomparison project (WETCHIMP),
791 *Biogeosciences*, 10, 753-788.

792 Myhre, G., and Coauthors, 2013 Anthropogenic and Natural Radiative Forcing, in: *Climate*
793 *Change 2013: The Physical Science Basis. Contribution of Working Group I to the Fifth*
794 *Assessment Report of the Intergovernmental Panel on Climate Change*, Cambridge
795 University Press, Cambridge, United Kingdom and New York, NY, USA

796 Oleson, K. and Coauthors, 2008: Improvements to the Community Land Model and their impact
797 on the hydrological cycle, *Journal of Geophysical Research: Biogeosciences*, 113, G01021,
798 <http://doi.org/10.1029/2007JG000563>.

799 Olin, S. and Coauthors, 2015: Soil carbon management in large-scale Earth system modelling:
800 implications for crop yields and nitrogen leaching, *Earth System Dynamics*, 6, 745-768.

801 Pan, S. and Coauthors, 2015: Responses of global terrestrial evapotranspiration to climate
802 change and increasing atmospheric CO₂ in the 21st century, *Earth's Future*, 3, 15-35.

803 Parton, W., Holland, E., Del Grosso, S., Hartman, M., Martin, R., Mosier, A., Ojima, D., and
804 Schimel, D., 2001: Generalized model for NO_x and N₂O emissions from soils, *Journal of*
805 *Geophysical Research: Atmospheres*, 106, 17403-17419.

806 Parton, W., Mosier, A., Ojima, D., Valentine, D., Schimel, D., Weier, K., and Kulmala, A. E.,
807 1996: Generalized model for N₂ and N₂O production from nitrification and denitrification,
808 *Global Biogeochemical Cycles*, 10, 401-412.

809 Parton, W. J., Hartman, M., Ojima, D., and Schimel, D., 1998: DAYCENT and its land surface
810 submodel: description and testing, *Global and planetary Change*, 19, 35-48.

811 Potter, C. S., Matson, P. A., Vitousek, P. M., and Davidson, E. A., 1996: Process modeling of
812 controls on nitrogen trace gas emissions from soils worldwide, *Journal of Geophysical*
813 *Research: Atmospheres*, 101, 1361-1377.

814 Potter, C. S., Randerson, J. T., Field, C. B., Matson, P. A., Vitousek, P. M., Mooney, H. A., and
815 Klooster, S. A., 1993: Terrestrial ecosystem production: a process model based on global
816 satellite and surface data, *Global Biogeochemical Cycles*, 7, 811-841.

817 Poulter, B. et al. 2017: Global wetland contribution to 2000–2012 atmospheric methane growth
818 rate dynamics, *Environ. Res. Lett.* **12** (2017) 094013. [https://doi.org/10.1088/1748-](https://doi.org/10.1088/1748-9326/aa8391)
819 [9326/aa8391](https://doi.org/10.1088/1748-9326/aa8391)

820 Prather, M. J., Holmes, C. D., and Hsu, J., 2012: Reactive greenhouse gas scenarios: Systematic
821 exploration of uncertainties and the role of atmospheric chemistry, *Geophysical Research*
822 *Letter*, 39, L09803, <https://doi.org/10.1029/2012GL051440>.

823 Prather, M. J. and Coauthors, 2015: Measuring and modeling the lifetime of nitrous oxide
824 including its variability, *Journal of Geophysical Research: Atmosphere*, 120, 5693–5705.

825 Randerson, J. T. and Coauthors, 2009: Systematic assessment of terrestrial biogeochemistry in
826 coupled climate–carbon models, *Global Change Biology*, 15, 2462-2484.

827 Rice, C. W. and Smith, M. S., 1982: Denitrification in no-till and plowed soils, Soil Science
828 Society of America Journal, 46, 1168-1173.

829 Richardson, A. D. and Coauthors, 2012: Terrestrial biosphere models need better representation
830 of vegetation phenology: results from the North American Carbon Program Site Synthesis,
831 Global Change Biology, 18, 566-584.

832 Rowlings, D., Grace, P., Scheer, C., and Liu, S., 2015: Rainfall variability drives interannual
833 variation in N₂O emissions from a humid, subtropical pasture, Science of The Total
834 Environment, 512, 8-18.

835 Saikawa, E. and Coauthors, 2014: Global and regional emissions estimates for N₂O,
836 Atmospheric Chemistry and Physics, 14, 4617-4641.

837 Saikawa, E., Schlosser, C., and Prinn, R., 2013: Global modeling of soil nitrous oxide emissions
838 from natural processes, Global Biogeochemical Cycles, 27, 972-989.

839 Saunio, M. and Coauthors, 2016: The global methane budget 2000–2012, Earth Syst. Sci. Data,
840 8, 697-751, <https://doi.org/10.5194/essd-8-697-2016>.

841 Schaefer, K. and Coauthors, 2012: A model-data comparison of gross primary productivity:
842 Results from the North American Carbon Program site synthesis, Journal of Geophysical
843 Research: Biogeosciences, 117, G03010, <http://doi.org/10.1029/2012JG001960>.

844 Schimel, D. and Coauthors, 2000: Contribution of increasing CO₂ and climate to carbon storage
845 by ecosystems in the United States, Science, 287, 2004-2006.

846 Schmidt, I., van Spanning, R. J., and Jetten, M. S., 2004: Denitrification and ammonia oxidation
847 by Nitrosomonas europaea wild-type, and NirK- and NorB-deficient mutants, Microbiology,
848 150, 4107-4114.

849 Schwalm, C. R. and Coauthors, 2010: A model-data intercomparison of CO₂ exchange across
850 North America: Results from the North American Carbon Program site synthesis, Journal of
851 Geophysical Research: Biogeosciences, 115, G00H05, <http://doi.org/10.1029/2009JG001229>.

852 Shevliakova, E. and Coauthors, 2009: Carbon cycling under 300 years of land use change:
853 Importance of the secondary vegetation sink, Global Biogeochemical Cycles, 23, GB2022,
854 <http://doi.org/10.1029/2007GB003176>.

855 Sitch, S. and Coauthors, 2015: Recent trends and drivers of regional sources and sinks of carbon
856 dioxide, Biogeosciences, 12, 653-679.

857 Smith, K. A. and Arah, J., 1990: Losses of nitrogen by denitrification and emissions of nitrogen
858 oxides from soils, Proceedings-Fertilizer Society, UK, 299.

859 Stocker, B. D., Roth, R., Joos, F., Spahni, R., Steinacher, M., Zaehle, S., Bouwman, L., and
860 Prentice, I. C., 2013: Multiple greenhouse-gas feedbacks from the land biosphere under
861 future climate change scenarios, *Nature Climate Change*, 3, 666-672.

862 Stöckli, R., Lawrence, D., Niu, G. Y., Oleson, K., Thornton, P. E., Yang, Z. L., Bonan, G.,
863 Denning, A., and Running, S. W., 2008: Use of FLUXNET in the Community Land Model
864 development, *Journal of Geophysical Research: Biogeosciences*, 113, G01025,
865 <http://doi.org/10.1029/2007JG000562>.

866 Thompson, R. L. and Coauthors, 2014: TransCom N₂O model inter-comparison – Part 2:
867 Atmospheric inversion estimates of N₂O emissions, *Atmospheric Chemistry and Physics*, 14,
868 6177–6194, <https://doi.org/10.5194/acp-14-6177-2014>.

869 Thornton, P. E. and Coauthors, 2009: Carbon-nitrogen interactions regulate climate-carbon cycle
870 feedbacks: results from an atmosphere-ocean general circulation model, *Biogeosciences*, 6,
871 2099-2120.

872 Thornton, P. E., Lamarque, J. F., Rosenbloom, N. A., and Mahowald, N. M., 2007: Influence of
873 carbon-nitrogen cycle coupling on land model response to CO₂ fertilization and climate
874 variability, *Global Biogeochemical Cycles*, 21, GB4018,
875 <http://doi.org/10.1029/2006GB002868>.

876 Tian, H. and Coauthors, 2015: Global methane and nitrous oxide emissions from terrestrial
877 ecosystems due to multiple environmental changes, *Ecosystem Health and Sustainability*, 1,
878 1-20.

879 Tian, H. and Coauthors, 2012: Century-scale responses of ecosystem carbon storage and flux to
880 multiple environmental changes in the southern United States, *Ecosystems*, 15, 674-694.

881 Tian, H. and Coauthors, 2016: The terrestrial biosphere as a net source of greenhouse gases to
882 the atmosphere, *Nature*, 531, 225-228.

883 Tian, H., Xu, X., Liu, M., Ren, W., Zhang, C., Chen, G., and Lu, C., 2010: Spatial and temporal
884 patterns of CH₄ and N₂O fluxes in terrestrial ecosystems of North America during 1979-2008:
885 application of a global biogeochemistry model, *Biogeosciences*, 7, 2673-2694.

886 Tian, H., Xu, X., Lu, C., Liu, M., Ren, W., Chen, G., Melillo, J., and Liu, J., 2011: Net
887 exchanges of CO₂, CH₄, and N₂O between China's terrestrial ecosystems and the atmosphere

888 and their contributions to global climate warming, *Journal of Geophysical Research:*
889 *Biogeosciences*, 116, G02011, <http://doi.org/10.1029/2010JG001393>.

890 Vuichard et al., Accounting for carbon and nitrogen interactions in a global terrestrial ecosystem
891 model: Multi-site evaluation of the ORCHIDEE model, in prep.

892 Wania, R. and Coauthors, 2013: Present state of global wetland extent and wetland methane
893 modelling: methodology of a model inter-comparison project (WETCHIMP), *Geoscientific*
894 *Model Development*, 6, 617-641.

895 Warszawski, L., Frieler, K., Huber, V., Piontek, F., Serdeczny, O., and Schewe, J., 2014: The
896 inter-sectoral impact model intercomparison project (ISI-MIP): project framework,
897 *Proceedings of the National Academy of Sciences*, 111, 3228-3232.

898 Wei, Y. and Coauthors, 2014: The North American Carbon Program Multi-scale Synthesis and
899 Terrestrial Model Intercomparison Project – Part 2: Environmental driver data, *Geosci.*
900 *Model Dev.*, 7, 2875-2893, <https://doi.org/10.5194/gmd-7-2875-2014>.

901 Winiwarter, W., Höglund-Isaksson, L., Klimont, Z., Schöpp, W., Amann, M., 2017: Technical
902 opportunities to reduce global anthropogenic emissions of nitrous oxide *Environ. Res. Letters*,
903 DOI 10.1088/1748-9326/aa9ec9

904 Wrage, N., Velthof, G., Van Beusichem, M., and Oenema, O.: Role of nitrifier denitrification in
905 the production of nitrous oxide, *Soil biology and Biochemistry*, 33, 1723-1732, 2001.

906 Xu-Ri, and Prentice I. C.: Terrestrial nitrogen cycle simulation with a dynamic global vegetation
907 model. *Global Change Biology*, 14, 1745-1764, 2008.

908 Xu, R., Tian, H., Lu, C., Pan, S., Chen, J., Yang, J., and Zhang, B., 2017: Preindustrial nitrous
909 oxide emissions from the land biosphere estimated by using a global biogeochemistry model,
910 *Climate of the Past*, 13, 977-990, <https://doi.org/10.5194/cp-13-977-2017>.

911 Xu, X., Tian, H., Chen, G., Liu, M., Ren, W., Lu, C., and Zhang, C., 2012: Multifactor controls
912 on terrestrial N₂O flux over North America from 1979 through 2010, *Biogeosciences*, 9,
913 1351-1366.

914 Yang, Q., Tian, H., Friedrichs, M. A., Hopkinson, C. S., Lu, C., and Najjar, R. G., 2015:
915 Increased nitrogen export from eastern North America to the Atlantic Ocean due to climatic
916 and anthropogenic changes during 1901–2008, *Journal of Geophysical Research:*
917 *Biogeosciences*, 120, 1046-1068.

918 Zaehle, S., Ciais, P., Friend, A. D., and Prieur, V., 2011: Carbon benefits of anthropogenic
919 reactive nitrogen offset by nitrous oxide emissions, *Nature Geoscience*, 4, 601-605.

920 Zaehle, S. and Friend, A., 2010: Carbon and nitrogen cycle dynamics in the O-CN land surface
921 model: 1. Model description, site-scale evaluation, and sensitivity to parameter estimates,
922 *Global Biogeochemical Cycles*, 24, GB1005, <http://doi.org/10.1029/2009GB003521>.

923 Zhang, B., Tian, H., Lu, C., Dangal, S. R. S., Yang, J., and Pan, S., 2017: Manure nitrogen
924 production and application in cropland and rangeland during 1860-2014: A 5-minute gridded
925 global data set for Earth system modeling. *Earth System Science Data Discussion*,
926 <https://doi.org/10.5194/essd-2017-11>.

927 Zhang, K., Peng C.H., Wang M., Zhou X.L., Li M.X., Wang K.F., Ding J.H., and Zhu Q.A.,
928 2017: Process-based TRIPLEX-GHG model for simulating N₂O emissions from global forests
929 and grasslands: Model development and evaluation. *Journal of Advances in Modeling Earth*
930 *Systems*, In revision.

931 Zhang, Y., Li, C., Zhou, X., and Moore, B., 2002: A simulation model linking crop growth and
932 soil biogeochemistry for sustainable agriculture, *Ecological Modelling*, 151, 75-108.

933 Zhu, Q. and Coauthors, 2014: Modelling methane emissions from natural wetlands by
934 development and application of the TRIPLEX-GHG model, *Geoscientific Model*
935 *Development*, 7, 981-999.

936 Zhuang, Q., Lu, Y., and Chen, M., 2012: An inventory of global N₂O emissions from the soils of
937 natural terrestrial ecosystems. *Atmospheric environment*, 47, 66-75.

938

939

940

941

942

943

944

945

946

947

948

949 **Figure Captions**

950 **Figure 1.** The framework of the N₂O Model Intercomparison project (NMIP).

951
952 **Figure 2.** Evolution of the major driving factors at the global level during 1901-2016. (a) Annual
953 temperature (°C, solid line) and annual precipitation (mm, dash line), (b) atmospheric CO₂
954 concentration (ppm), (c) cropland area (million km²), (d) N deposition (Tg N yr⁻¹), (e) N
955 fertilizer application (Tg N yr⁻¹) during 1900-2013, and (f) manure N production (Tg N yr⁻¹).

956
957 **Figure 3.** Spatial distribution of N deposition (a, d, g, j; g N m⁻² yr⁻¹), N fertilizer application (b,
958 e, h, k; g N m⁻² yr⁻¹), and manure N production (c, f, i, l; g N m⁻² yr⁻¹) in 1860 (1st row),
959 1900 (2nd row), 1950 (3rd row), and 2015 (4th row).

960
961 **Figure 4.** Model simulation experimental designs (Note: S0: reference (baseline); S1:
962 CLIM+CO₂+LCLU+NDEP+NFER+MANN; S2: CLIM+ CO₂+LCLU+NDEP+NFER; S3:
963 CLIM+ CO₂+LCLU+NDEP; S4: CLIM+ CO₂+LCLU; S5: CLIM+ CO₂; S6: CLIM). CLIM:
964 climate, CO₂: atmospheric CO₂, LCLU: land cover and land use change, NDEP: N deposition,
965 NFER: N fertilizer use, and MANN: manure N use.

966
967 **Figure 5.** Interannual variations in N₂O emissions from global terrestrial ecosystems during
968 1861-2015 as estimated by the average of three process-based models (DLEM, O-CN, and
969 VISIT). The gray shades denote ± 1 standard deviation.

970
971 **Figure 6.** Spatial patterns and the latitudinal variations of mean annual N₂O emissions as
972 represented by the mean estimates from DLEM, VISIT, and O-CN models in the (a) 1860s, (b)
973 1900s, (c) 1950s, and (d) 2001-2015. The pie charts indicate the relative contributions of natural
974 vegetation (blue) and cropland (red) to the total N₂O emissions. The gray shades denote ± 1
975 standard deviation.

976
977 **Figure 7.** Decadal N₂O emissions (Tg N yr⁻¹) from the natural ecosystems (blue lines) and
978 cropland (red lines) in 14 regions (region delineation is from the Global Carbon Project global
979 CH₄ budget synthesis, Saunio et al., 2016). N₂O emissions are represented by the average of
980 DLEM, VISIT, and O-CN model simulations. The error bars denote ± 1 standard deviation.

981

982 **Table 1.** Summary of the NMIP driving forces
 983

Data name	Period	Temporal resolution	Spatial resolution	Sources	Variables
Climate	1901-2015	6-hourly	0.5°	CRU-NCEP	Incoming longwave / shortwave radiation, air humidity, pressure, precipitation, temperature, and wind speed
CO ₂	1860-2015	Monthly	0.5°	NCAR	CO ₂ concentration
N deposition	1860-2015	Yearly	0.5°	Eyring et al. (2013)	NH _x -N and NO _y -N deposition
N Fertilizer use	1860-2014	Yearly	0.5°	Lu and Tian (2017)	N fertilizer use rate in cropland
Manure N input	1860-2014	Yearly	0.5°	Zhang et al. (2017)	Manure N production
Potential vegetation	One time	One time	0.5°	SYNMAP	Fraction of natural vegetation types
Cropland	1860-2015	Yearly	0.5°	HYDE 3.2	Cropland fraction

984 Note: Detailed descriptions of the major NMIP model input datasets have been provided in
 985 previous publications or online documents. Here we only provide a brief description of sources
 986 and spatiotemporal patterns of these datasets.

987 **Table 2.** Participating models

Model	Full name	Contact	Affiliation	Citation
CLM-CN	Community land model - CN	Eri Saikawa	Emory University, USA	Saikawa et al. (2013)
DLEM	Dynamic Land Ecosystem Model	Hanqin Tian	Auburn University	Tian et al. (2015) Xu et al. (2017)
LM3V-N	Land Model 3V-N	Stefan Gerber	University of Florida	Huang and Gerber (2015)
LPJ-GUESS	Lund-Potsdam-Jena General Ecosystem Simulator	Stefan Olin/ Almut Arneth	Lund University, Sweden/KIM, Dept. Atmospheric Environmental Research, Germany	Olin et al. (2015); Xu-Ri and Prentice (2008)
LPX-Bern	Land Processes and eXchanges model - Bern	Sebastian Lienert/ Fortunat Joos	Institute for Climate and Environmental Physics, University of Bern, Switzerland	Stocker et. al. (2013) Xu-Ri and Prentice (2008)
O-CN	ORCHIDEE-CN	Sönke Zaehle	Max Planck Institute for Biogeochemistry	Zaehle et al. (2011)
ORCHIDEE	Organising Carbon and Hydrology In Dynamic Ecosystems	Nicolas Vuichard	IPSL – LSCE, France	Vuichard et al. (in prep)
ORCHIDEE-CNP	Organising Carbon and Hydrology In Dynamic Ecosystems-CNP	Jinfeng Chang/ Daniel Goll	IPSL – LSCE, France	Goll et al., 2017
TRIPLEX-GHG	TRIPLEX-GHG	Changhui Peng	University of Quebec at Montreal, Canada	Zhu et al. (2014); Zhang et al. (2017)
VISIT	Vegetation Integrated Simulator for Trace-gases	Akihiko Ito	National Institute for Environmental Studies, Japan	Inatomi et al. (2010); Ito and Inatomi (2012)

Table 3. Model characteristics in simulating major N cycling processes

	CLM-CN	DLEM	LM3V-N	LPJ -GUESS	LPX-Bern	O-CN	ORCHIDEE	ORCHIDEE -CNP	TRIPLEX-GHG	VISIT
Open N cycle ¹	yes	yes	yes	yes	yes	yes	yes	yes	yes	yes
C-N coupling	yes	yes	yes	yes	yes	yes	yes	yes	yes	yes
N pools ²	(13, 3, 4)	(6, 6, 8)	(6, 4, 3)	(5, 6, 11)	(4,3,8)	(9, 6, 9)	(9, 6, 9)	(9, 6, 9)	(3, 9, 4)	(4, 1, 4)
Demand and supply-driven Plant N uptake	yes	yes	yes	yes	yes	yes	yes	yes	yes	yes
N allocation ³	Dynamic	Dynamic	Dynamic	Dynamic	Dynamic	Dynamic	Dynamic	Dynamic	Dynamic	Dynamic
Nitrification	$f(T, SWC)$	$f(T, SWC, C_{NH4})$	$f(T, SWC, C_{NH4})$	$f(T, SWC, C_{NH4})$	$f(T, SWC, C_{NH4})$	$f(T, SWC, pH, C_{NH4})$	$f(T, SWC, pH, C_{NH4})$	$f(T, SWC, pH, C_{NH4})$	$f(pH, C_{NH4}, T, SWC)$	$f(T, SWC, pH, C_{NH4})$
Denitrification	$f(T, SWC, C_{NO3})$	$f(T, clay, Rh, C_{NO3})$	$f(T_{soil}, Rh, SWC, C_{NH4}, C_{NO3})$	$f(T, Rh, SWC, C_{NO3})$	$f(T, SWC, R_{mb}, C_{NO3})$	$f(T, SWC, pH, R_{mb}, C_{NO3})$	$f(T, SWC, pH, denitrifier, C_{NO3})$	$f(T, SWC, pH, R_{mb}, C_{NO3})$	$f(DOC, C_{NO3}, pH, T_{soil})$	$f(SWC, Rh, C_{NO3})$
Mineralization, immobilization	$f(C:N)$	$f(C:N)$	$f(C_{NO3}, C_{NH4})$	$f(C:N)$	$f(C:N)$	$f(C:N)$	$f(C:N)$	$f(C:N)$	$f(C:N)$	$f(C:N)$
N leaching	$f(runoff)$	$f(runoff)$	$f(runoff)$	$f(runoff)$	$f(runoff)$	$f(runoff, clay)$	$f(runoff)$	$f(runoff)$	$f(runoff)$	$f(runoff)$
NH ₃ volatilization	$f(C_{NH4})$	$f(pH, T, SWC, C_{NH4})$	$f(pH, T, SWC, C_{NH4})$	$f(pH, T, SWC, C_{NH4})$	$f(pH, T, SWC, C_{NH4})$	$f(pH, C_{NH4})$	$f(pH, C_{NH4})$	$f(pH, C_{NH4})$	$f(pH, C_{NH4})$	$f(pH, T, SWC, C_{NH4})$
Plant N turnover ⁴	Dynamic	Dynamic	Dynamic	Dynamic	Dynamic	Dynamic	Dynamic	Dynamic	Dynamic	Dynamic
N resorption	$f(C:N)$	$f(C:N)$	fixed	Crop: dynamic, the rest: fixed	$f(N_{leaf})$	fixed	$f(N_{leaf})$	fixed	$f(C:N)$	fixed
N fixation	$f(NPP)$	Fixed	$f(C_{NH4}, C_{NO3}, light, plant demand)$	$f(ET)$	<i>Implied by mass balance</i>	$f(C_{cost}, C_{root})$	$f(ET)$	$f(NPP)$	$f(biomass)$	$f(ET)$
N fertilizer use	no	yes	yes	yes	yes	yes	yes	yes	yes	yes
Manure N use	no	yes	yes	yes	no	no	yes	yes	no	yes
N deposition	yes	yes	yes	yes	yes	yes	yes	yes	yes	yes

989 Note: ¹ “open” denotes that excess N can be leached from the system; ² numbers of N pools (vegetation pools, litter pools, soil pools); ³ Dynamic denotes time-varied N allocation
990 ratio to different N pools; ⁴ turnover time for various vegetation nitrogen pools. T: soil temperature; Clay: soil clay fraction; ET: evapotranspiration; Biomass: vegetation carbon;
991 NPP: net primary production; Nleaf: leaf N concentration; Runoff: soil surface and drainage runoff; Ccost: carbon cost during N₂ fixation; SWC: soil water content; denitrifier: soil
992 denitrifier biomass; Rh: soil heterogeneous respiration.

993
994
995
996

Table 4. List of nitrogen and carbon variables provided by NMIP models

Name of Variables	Unit	Frequency	Level
Nitrogen Fluxes:			
N ₂ O flux, Biological N fixation, Plant N uptake (sum of ammonium and nitrate), Net N mineralization, Nitrification rate, Denitrification rate, N leaching (DIN, DON, PON or total N leaching), NH ₃ volatilization	kg N m ⁻² s ⁻¹	Monthly (1980-2015) Annual (1860-2015)	Grid- and biome-levels
Nitrogen Pools:			
N in Vegetation, N in Above-ground Litter Pool, N in Soil (including below-ground litter), N in Products pools	kg N m ⁻²	Annual (1860-2015)	Grid-levels
Carbon Fluxes:			
Gross Primary Production, Autotrophic (Plant) Respiration, Net Primary Production, Heterotrophic Respiration	kg C m ⁻² s ⁻¹	Monthly (1980-2015) Annual (1860-2015)	Grid- and biome-levels
Carbon Pools:			
C in Vegetation, C in Above-ground Litter Pool, C in Soil (including below-ground litter), C in Products pools, C in Vegetation	kg C m ⁻²	Annual (1860-2015)	Grid-level Biome-level (vegetation C)

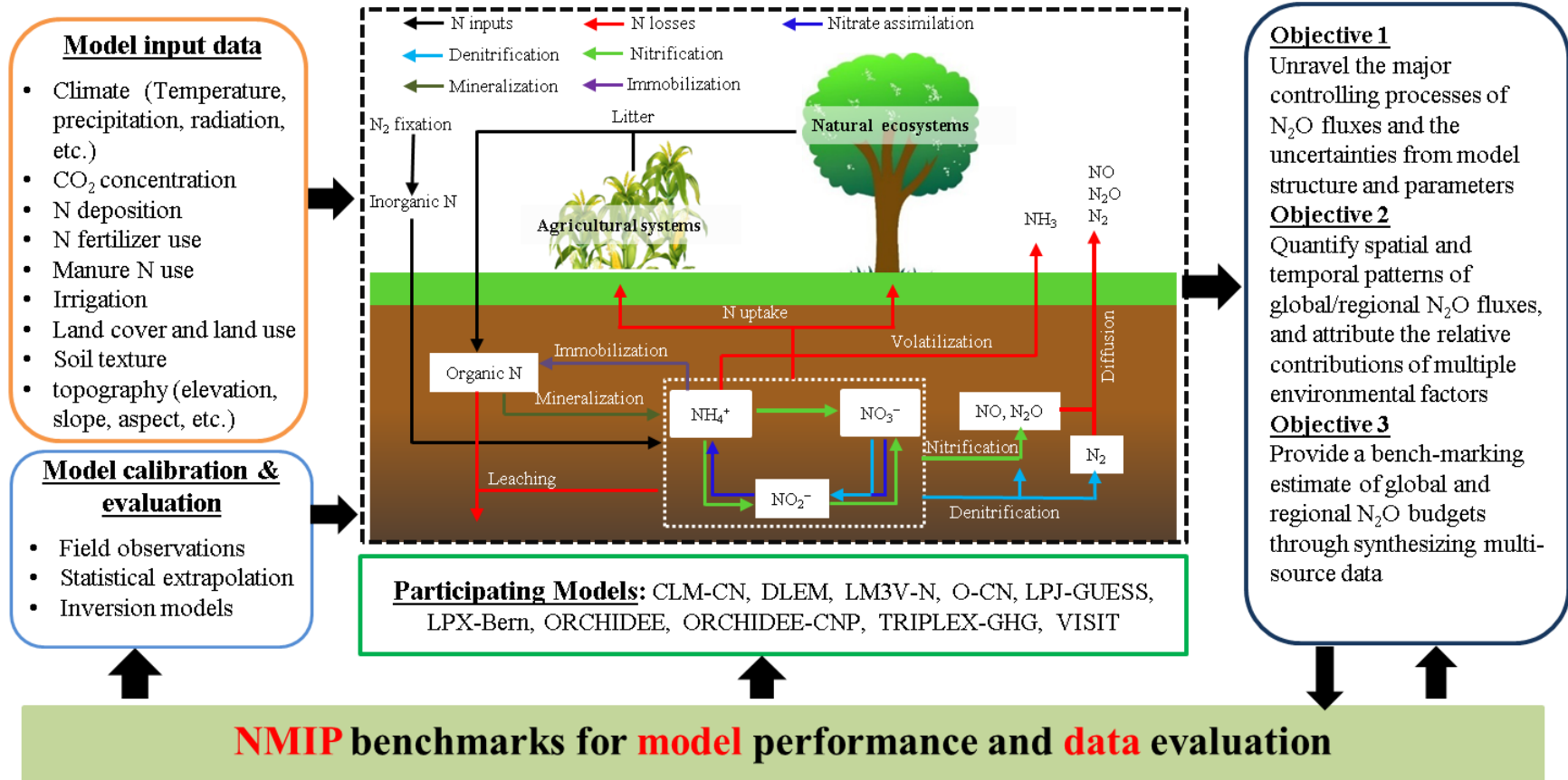
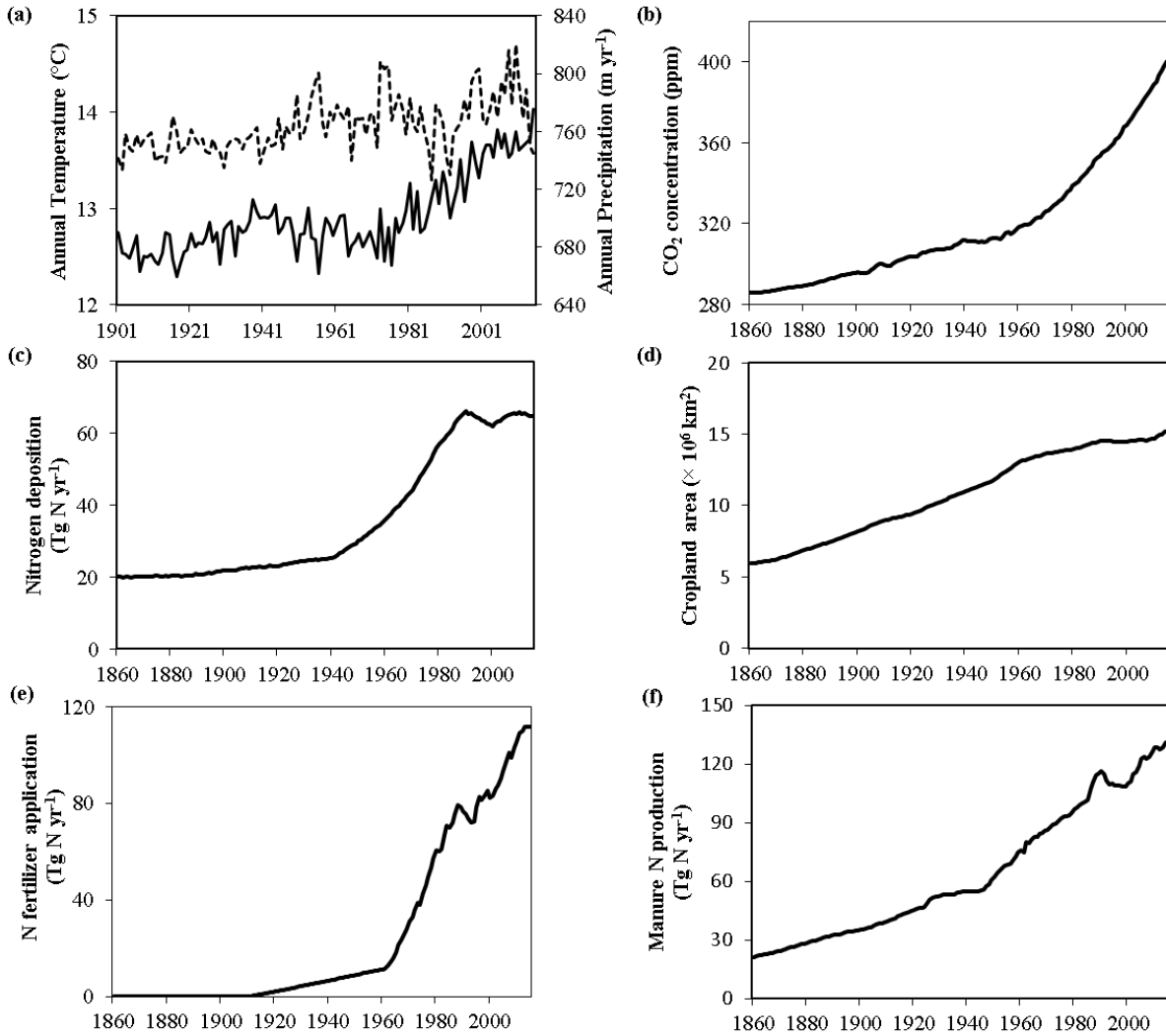
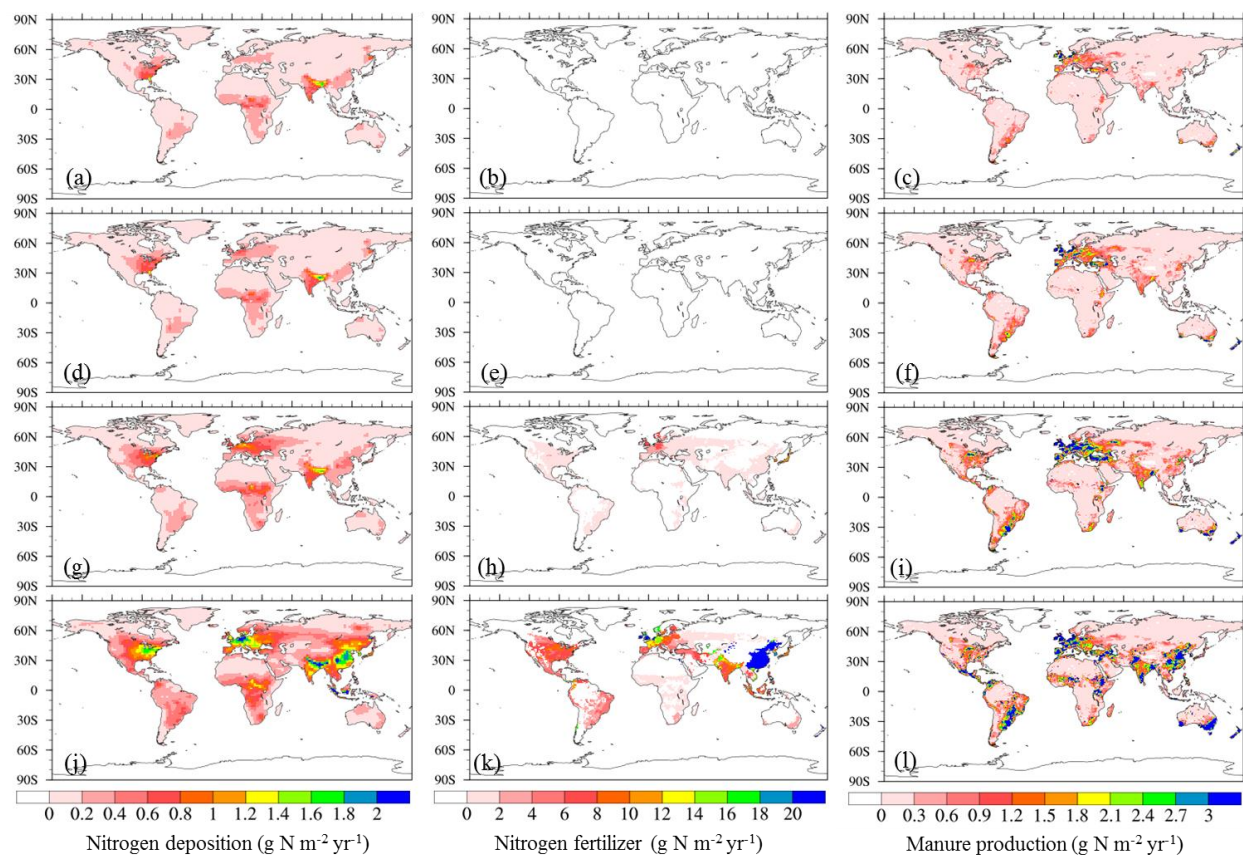


Figure 1. The framework of the N₂O Model Intercomparison project (NMIP)



1001
 1002 **Figure 2.** Evolution of the major driving factors at the global level during 1901-2016. (a) Annual
 1003 temperature (°C, solid line) and annual precipitation (mm, dash line), (b) atmospheric CO₂
 1004 concentration (ppm), (c) cropland area (million km²), (d) N deposition (Tg N yr⁻¹), (e) N
 1005 fertilizer application (Tg N yr⁻¹) during 1900-2013, and (f) manure N production (Tg N yr⁻¹).

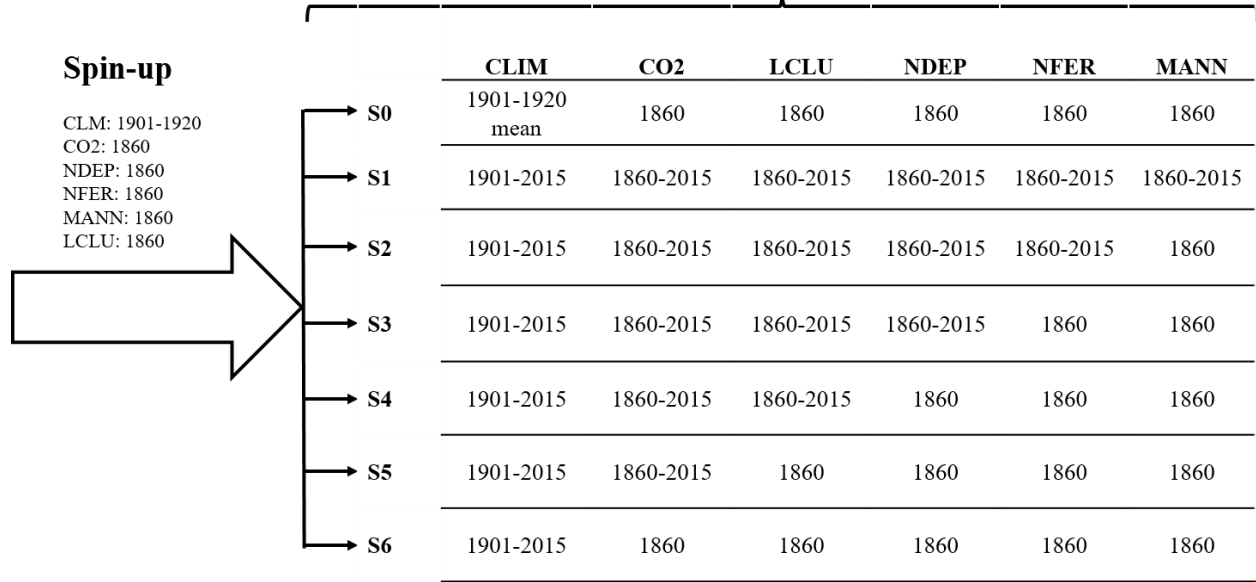
1006
1007



1009

1010 **Figure 3.** Spatial distribution of N deposition (a, d, g, j; g N m⁻² yr⁻¹), N fertilizer application (b,
1011 e, h, k; g N m⁻² cropland yr⁻¹), and manure N production (c, f, i, l; g N m⁻² yr⁻¹) in 1860 (1st row),
1012 1900 (2nd row), 1950 (3rd row), and 2015 (4th row).
1013

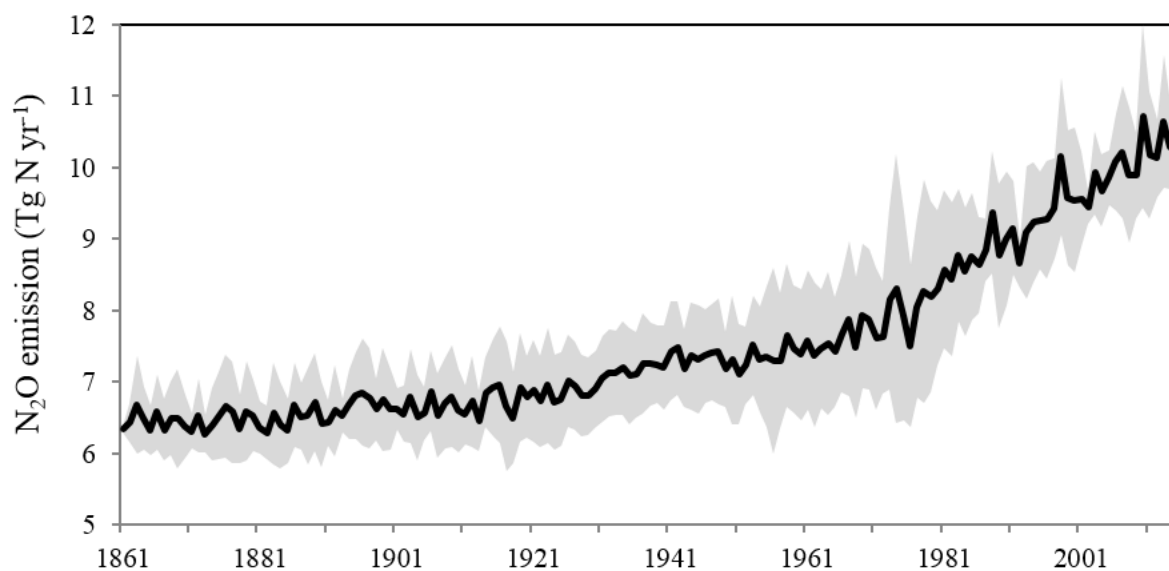
Transient Run (1860-2015)



1014
1015

1016 **Figure 4.** Model simulation experimental designs (Note: S0: reference (baseline); S1:
1017 CLIM+CO₂+LCLU+NDEP+NFER+MANN; S2: CLIM+ CO₂+LCLU+NDEP+NFER; S3:
1018 CLIM+ CO₂+LCLU+NDEP; S4: CLIM+ CO₂+LCLU; S5: CLIM+ CO₂; S6: CLIM). CLIM:
1019 climate, CO₂: atmospheric CO₂, LCLU: land cover and land use change, NDEP: N deposition,
1020 NFER: N fertilizer use, and MANN: manure N use

1021



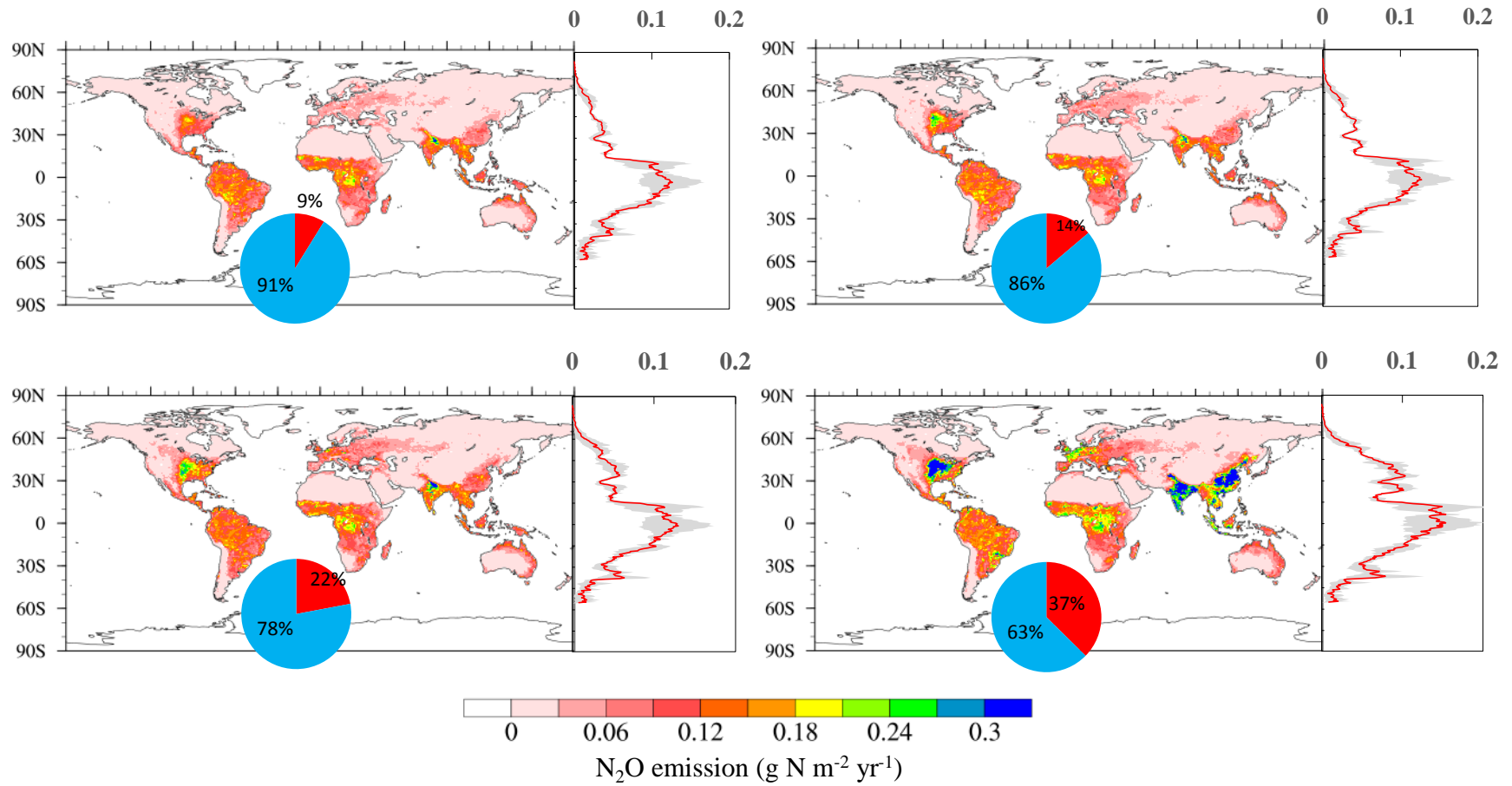
1022

1023 **Figure 5.** Interannual variations in N₂O emissions from global terrestrial ecosystems during
1024 1861-2015 as estimated by the average of three process-based models (DLEM, O-CN, and
1025 VISIT). The gray shades denote ± 1 standard deviation.

1026

1027

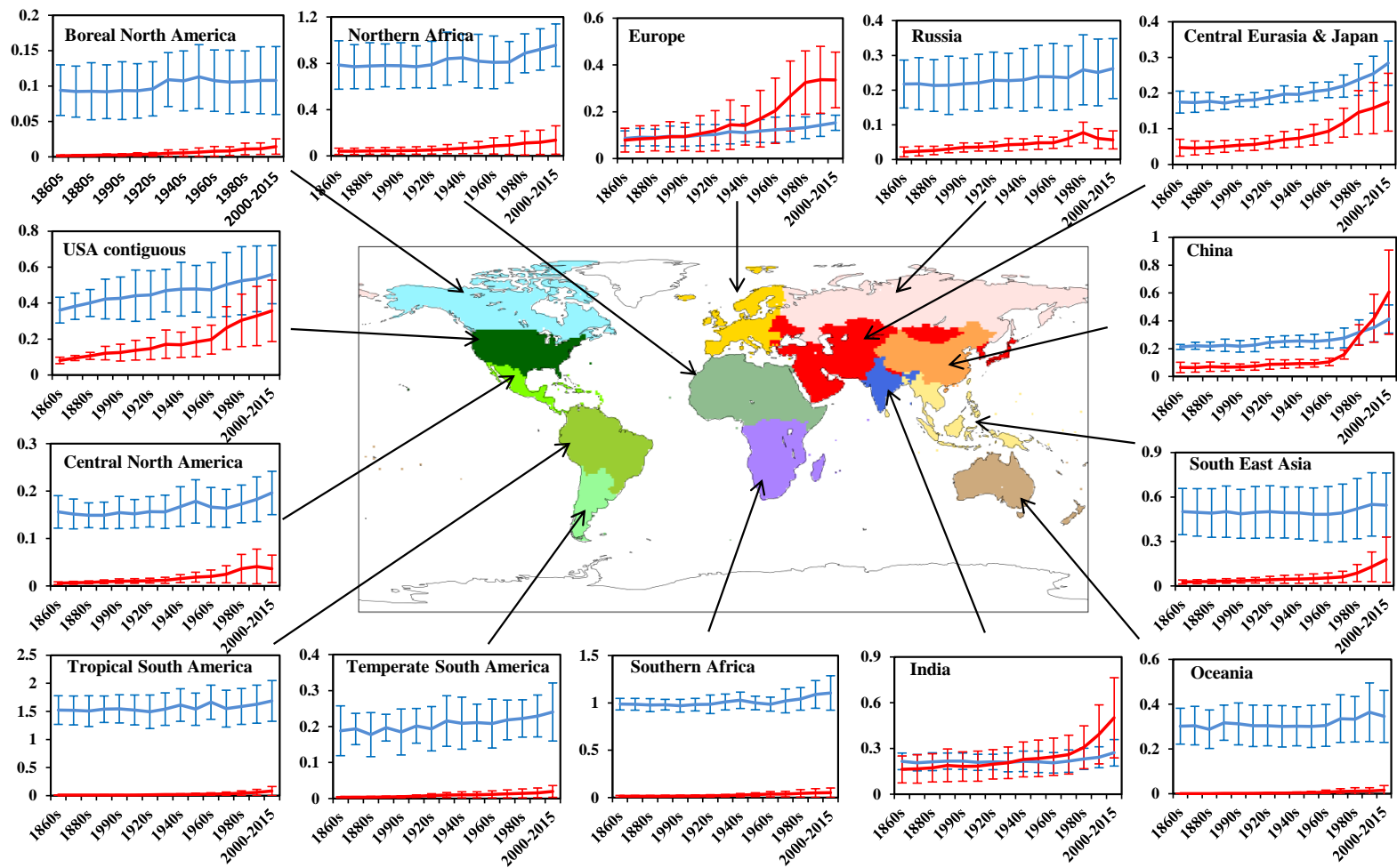
1028



1029

1030 **Figure 6.** Spatial patterns and the latitudinal variations of mean annual N_2O emissions as represented by the mean estimates from
 1031 DLEM, VISIT, and O-CN models in the (a) 1860s, (b) 1900s, (c) 1950s, and (d) 2001-2015. The pie charts indicate the relative
 1032 contributions of natural vegetation (blue) and cropland (red) to the total N_2O emissions. The gray shades denote ± 1 standard deviation.
 1033

1034



1035

1036

1037 **Figure 7.** Decadal N₂O emissions (Tg N yr⁻¹) from the natural ecosystems (blue lines) and cropland (red lines) in 14 regions (region
 1038 delineation is from the Global Carbon Project global CH₄ budget synthesis, Saunio et al., 2016). N₂O emissions are represented by
 1039 the average of DLEM, VISIT, and O-CN model simulations. The error bars denote ± 1 standard deviation.